Ph.D. Dissertation of Physics

Semiconducting Carbon Nanotube Transistors for the Real-time Monitoring of Cellular Transport and Their Application to Drug Evaluation

세포 수송의 실시간 모니터링을 위한 반도체 탄소나노튜브 트랜지스터와 이를 이용한 약물 평가에 관한 연구

August 2019

Seoul National University
Graduate School of Natural Sciences
Department of Physics and Astronomy

PHAM BA VIET ANH

Semiconducting Carbon Nanotube Transistors for the Real-time Monitoring of Cellular Transport and Their Application to Drug Evaluation

Professor Seunghun Hong

Submitting a Ph.D. Dissertation of Physics

June 2019

Seoul National University

Graduate School of Natural Sciences

Department of Physics and Astronomy

PHAM BA VIET ANH

Confirming the Ph.D. Dissertation written by Pham Ba Viet Anh

June 2019

Chair	Takhee Lee	(Seal)
Vice Chair	Seunghun Hong	(Seal)
Examiner	Sungchul Hohng	(Seal)
Examiner	Hye Yoon Park	(Seal)
Examiner	Kwang Heo	(Seal)

Abstract

Pham Ba Viet Anh
Department of Physics and Astronomy
Graduate School of Natural Sciences
Seoul National University

Cellular transport plays critical functions for the development and proliferation of cells. This process regulates the entry and release of biomaterials such as ions, neurotransmitters, proteins for cells. Because of its important roles, the cellular transport has been considered the key of drug development and medical therapy. In this dissertation, cellular transport such as Ca^{2+} influx, dopamine and cytokine release could be monitored in a real-time manner by using biosensors based on semiconducting carbon nanotube (sCNT) transistors. Furthermore, these biosensors have been utilized to quantitatively evaluate the effects of antihistamine, antipsychotic and anti-inflammatory drugs. The quantitative and real-time evaluation capability of our strategy would promise versatile applications such as drug screening and nanoscale biosensor researches.

Firstly, we discussed the quantitative electrophysiological monitoring of histamine and antihistamine drug effects on live cells via reusable sensor platforms based on sCNT transistors. This method enabled us to monitor the real-time electrophysiological responses of a single HeLa cell to histamine with different concentrations. The electrophysiological responses were attributed to the activity of histamine type 1 receptors on a HeLa cell membrane by histamine. Furthermore, the effects of antihistamine drugs such as cetirizine or chlorphenamine on the electrophysiological activities of HeLa cells were also quantitatively evaluated. Significantly, we utilized only a single device to monitor the responses of multiple HeLa cells to each drug, which allowed us to quantitatively analyze the antihistamine drug effects on

live cells without errors from the device-to-device variation in device characteristics.

Secondly, we developed floating electrode-based carbon nanotube biosensors for the monitoring of antipsychotic drug effects on the dopamine release from PC12 cells under potassium stimulation. Here, sCNT transistors with floating electrodes were functionalized with 2,2'-azino-bis(3-ethylbenzothiazoline-6-sulfonic acid) ($ABTS^{\bullet}$) radicals by Nafion films. This method allows us to build selective biosensors for dopamine detection with a detection limit down to 10 nM even in the presence of other neurotransmitters such as glutamate and acetylcholine, resulting from the selective interaction between $ABTS^{\bullet}$ radicals and dopamine. The sensors were also utilized to monitor the real-time release of dopamine from PC12 cells upon the stimulation of high-concentrated potassium solutions. Significantly, the antipsychotic effects of pimozide on the dopamine release from potassium-stimulated PC12 cells could also be evaluated in a concentration-dependent manner by using the sensors.

Lastly, we reported modified floating electrode-based sCNT sensors for the detection of tumor necrosis factor α (TNFα), a pro-inflammatory cytokine related with inflammatory bowel disease (IBD). Here, antibodies (anti-TNFα) were immobilized on the floating electrodes of sCNT sensors, enabling selective and real-time detection of TNFα among various cytokines linked to IBD. This sensor was able to detect the concentrations of TNFα with a detection limit of 1 pg/L, allowing to quantitatively monitor the anti-inflammatory effect of a drug, lupeol, on the activation of the LPS-induced nuclear factor κB signaling in mouse macrophage Raw 264.7 cells.

Keyword: semiconducting carbon nanotube, field-effect transistor, floating electrode, real-time monitoring, living cell, drug evaluation.
Student Number: 2014-30847

Table of Contents

Chapter 1. Introduction 1

1.1. Cellular transport 1

1.2. Conventional methods for the monitoring of cellular transport 3

1.3. Monitoring of cellular transport using sCNT transistors 5

1.4. Fabrication procedure of sCNT transistors 8

1.5. Basic characteristics of sCNT transistors 10

1.6. References 12

Chapter 2. Reusable sCNT transistors for the evaluation of antihistamine drugs via Ca^{2+} influx into HeLa cells 15

2.1. Introduction 15

2.2. Characteristics of reusable sensors 18

2.3. Monitoring of histamine-induced Ca^{2+} influx into HeLa cells 19

2.4. Effect monitoring of antihistamine drugs on histamine-induced Ca^{2+} influx 23

2.5. Summary 27

2.6. References 28

Chapter 3. Nafion-radical films on sCNT transistors for the evaluation of antipsychotic drugs via dopamine release from PC12 cells 31

3.1. Introduction 31

3.2. Characteristics of NRC sensors 33

3.3. Discrimination of dopamine by NRC sensors 35

3.4. Real-time monitoring of K^+-evoked dopamine release from PC12 cells using NRC sensors 40

3.5. Monitoring antipsychotic effects on K^+-evoked dopamine release from PC12 cells by NRC sensors 43

3.6. Summary 45

3.7. References 46

Chapter 4. Modified floating electrode-based sCNT transistors for the evaluation of anti-inflammatory effects via TNFα secretion from Raw 264.7 cells.....50
4.1. Introduction 50
4.2. Characteristics of TNF sensors.....53
4.3. Detection of TNFα by using TNF sensors.....55
4.4. Monitoring the effect of anti-inflammatory on the NF-κB signaling pathway.....59
4.5. Summary.....61
4.6. References 62
Chapter 5. Conclusions 65
Acknowledgement.....67

List of Figures

Figure 1.1. Schematic diagrams illustrating three main types of membrane transport proteins. 1

Figure 1.2. Single-walled CNT structures with different chirality. 5

Figure 1.3. Plausible sensing mechanisms of biosensors based on *p*-type sCNT transistors. 6

Figure 1.4. Schematic diagram showing the fabrication procedure of sCNT transistors. 8

Figure 1.5. Topography image of sCNT transistors with three floating electrodes using two different CNT assembling methods. 10

Figure 1.6. Liquid gating effect of a sCNT transistor measured in a buffer solution.....11

Figure 2.1. Schematic diagram depicting an experimental procedure for the monitoring of Ca^{2+} influx into a cell. 16

Figure 2.2. Microscopic image showing a Hela cell captured by using a microcapillary on a reusable sensor. 18

Figure 2.3. Quantitative electrophysiological monitoring of the effect of histamine drug on HeLa cells. 19

Figure 2.4. Repeated measurements for the responses of a single reusable sensor to multiple Hela cells during the injection of 100 mM histamine. 21

Figure 2.5. Quantitative electrophysiological monitoring of antihistamine drug effects using reusable sensors. 23

Figure 3.1. Schematic diagram depicting preparatory processes for the detection of dopamine released from living PC12 cells by using an NRC sensor. 32

Figure 3.2. Characterization of a Nafion-radical hybrid film on a floating electrode-based CNT sensor. 33

Figure 3.3. Responses of an NRC sensor to the presence of neurotransmitter solutions. 35
Figure 3.4. Responses of three different sCNT sensors to the presence of dopamine solutions. 37
Figure 3.5. Quantitative monitoring of dopamine release from living PC12 cells under the stimulation of K^+ solutions. 40
Figure 3.6. Evaluation of the effects of pimozide on K^+-evoked dopamine release from PC12 cells. 43
Figure 4.1. Schematic diagram depicting the preparatory procedure of TNF sensors for TNFα detection. 51
Figure 4.2. Characterization of a TNF sensor based on a CNT-FET sensor with floating electrodes. 53
Figure 4.3. Responses of TNF sensors to the addition of cytokine solutions. 55
Figure 4.4. Real-time measurements of electrical currents in sensors in response to the addition of TNFα solutions. 56
Figure 4.5. Evaluation of the inhibiting effect of lupeol on the LPS-induced NF-κB signaling pathway. 59

Chapter 1. Introduction

1.1. Cellular transport

Cellular transport refers to the movement of substances such as ions, neurotransmitters and proteins across the plasma membrane of a cell. The process is necessary for the uptake of nutrients, the elimination of wastes, and cell signaling [1,2]. The cell membrane is composed of a phospholipid bilayer which can allow hydrophobic and small polar molecules such as oxygen and water to easily diffuse through by selective permeability. Whereas, ions and some molecules such as proteins cannot pass through the phospholipid bilayer because of their charge and large size. The transport of ions, large molecules and hydrophilic molecules is regulated by specific membrane transport proteins in the cell membrane. Therefore, the activities of membrane transport proteins can be evaluated via the monitoring of cellular transport. The membrane transport proteins embed in and bridge the phospholipid bilayer forming gates which can assist the transport of such substances between the exterior and cytosol of the cells. Based on functional and operating differences, the membrane transport proteins are classified to three main types including channels, transporters and pumps (Figure 1.1) [3].

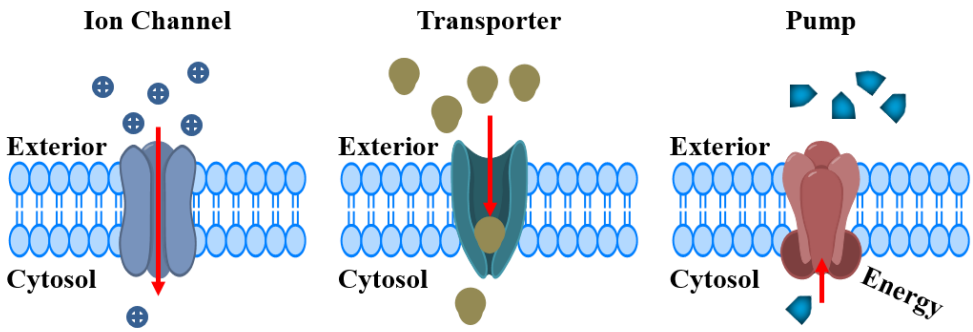

Figure 1.1. Schematic diagrams illustrating three main types of membrane transport proteins.

Ion channels form passageways across the cell membrane to transport ions down concentration or electrochemical gradients. The ion channels play crucial roles in the maintenance of membrane potential and the responses of electrophysiological activities. On the other hand, transporters bind to molecules, resulting in their conformational changes to transport these molecules across the cell membrane. Pumps use energy from ATP hydrolysis to transport substances such as ions or molecules across the cell membrane against concentration or electrochemical gradients. Since membrane transport proteins play key functions and roles for cell metabolism and proliferation, the membrane transport proteins are targets for new drug discovery and medical treatments.

1.2. Conventional methods for the monitoring of cellular transport

Conventional methods such as fluorescence assays, enzyme-linked immunosorbent assay (ELISA) technique, cyclic voltammetry and patch clamp have been utilized extensively to monitor cellular transport. However, these techniques have their own limitations. For example, fluorescence assays could be used to evaluate the activities of Ca^{2+} channels by the measurements of cytosolic Ca^{2+} concentrations via fluorescent probe signals [4,5]. However, fluorescent signal intensity can decay overtime, resulting in the difficulty of quantitative evaluation. Moreover, labeling processes required time-consuming steps. Another optical method is ELISA technique, which is mostly used to detect antigens in liquid samples such as cell supernatants and serums [6,7]. ELISA technique bases on the specific interactions between antibody and target antigen. Therefore, the ELISA technique requires multi-step manipulation and this is an indirect monitoring method.

Meanwhile, electrical methods such as cyclic voltammetry and patch clamp have exhibited outstanding performances in the monitoring of cellular transport. Based on redox processes on a working electrode, cyclic voltammetry can detect redox substances [8,9]. However, electrodes could be contaminated by the products of electrochemical reactions or agents in an ambient environment, resulting in the dependence of signals on experimental conditions and the difficulty of data estimation. Moreover, the detection limit of common electrochemical techniques is only at a micromolar level. The patch clamp methods exhibit high temporal and spatial resolution for the monitoring of electrophysiological activities in a cell [5,10]. This method allows us to monitor the activities of ion channels by the recording of ion currents across a cell membrane. For a measurement, a microelectrode forms a high resistance seal with the cell membrane. Therefore, the operation of this method requires complicated manipulations and invasive processes.

Furthermore, the patch clamp methods could measure an ion flux only at a specific location of a cell membrane rather than the electrical potential of the whole cell membrane, and, thus, it could only monitor the partial intracellular electrical signal pathways.

1.3. Monitoring of cellular transport using sCNT transistors

Various label-free techniques have been developed to overcome the drawbacks of conventional methods while still maintaining a high sensitivity and selectivity. For example, nanoscale devices based on CNTs have been utilized to monitor the activities of various cells [11-14].

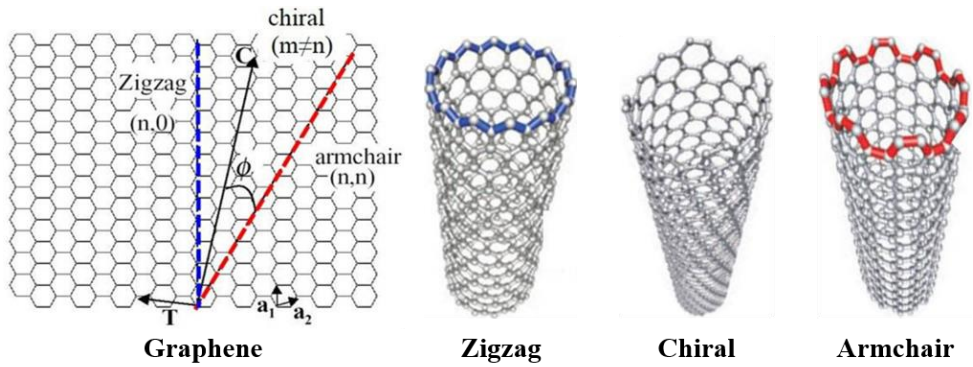

Figure 1.2. Single-walled CNT structures with different chirality.

CNTs (Figure 1.2) formed by the rolling-up of graphene sheets possess many notable properties such as high resistivity, high current density, high mobility, high tensile strength. Depending on the rolling-up direction of the graphene sheets, CNTs are either metallic or semiconducting [15]. Field-effect transistor (FET) devices based on sCNT with advantages such as high performance, versatile applications and real-time measurements allow us to monitor cellular transport processes and apply to various fields such as research tool development and drug screening. The successful development of CNT-FET devices for the detection of biomaterials shows that CNT-FET sensors have been considered as a potential candidate for the quantitative monitoring of cellular transport [16-18]. Moreover, it also indicates that a CNT-FET device functionalized with compatible materials could be used as an effective tool for the biomaterial detection and drug screening.

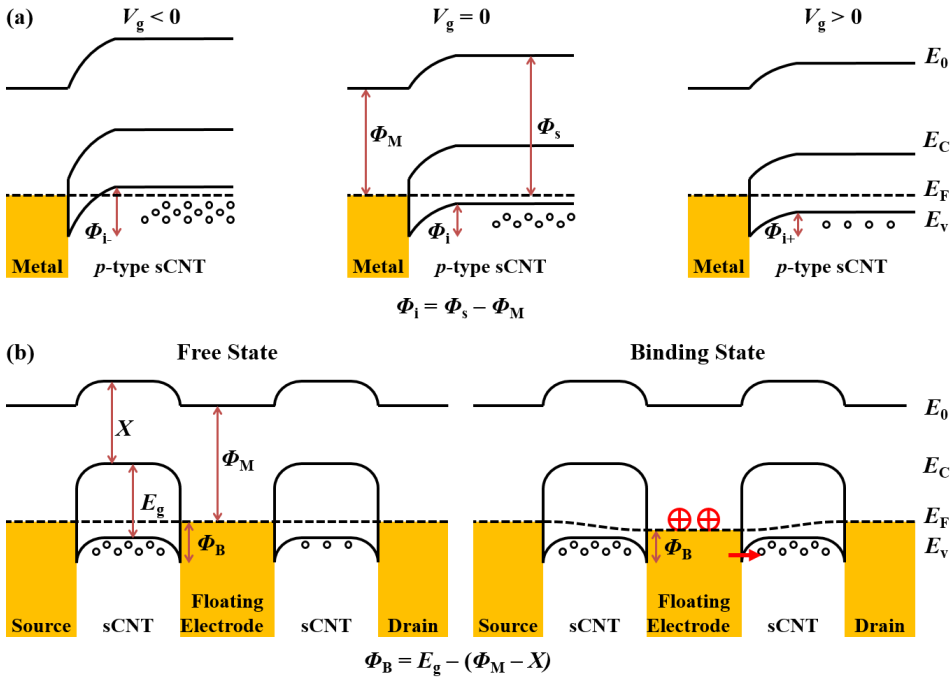

Figure 1.3. Plausible sensing mechanisms of biosensors based on p-type sCNT transistors. (a) Electrostatic gating effects. (b) Schottky barrier modulation.

The sensing mechanisms of sCNT biosensors have been suggested to be mainly associated with electrostatic gating effects and Schottky barrier modulation [19]. Electrostatic gating effects can be used to explain the mechanism of sensors with passivated metal-CNT contact regions. Figure 1.3(a) illustrates electrostatic gating effects on the conductance of *p*-type sCNT transistors. Built-in energy Φ_i is an energy barrier against the diffusion of hole carriers from the sCNT to the metal [20]. Φ_i can be modulated by the application of a gate voltage bias V_g. Negative gate voltages ($V_g < 0$) induce the accumulation of hole carriers in the CNTs via the elevation of energy bands, resulting in the conductance increase of the CNT transistor. Conversely, positive gate voltages ($V_g > 0$) reduce the energy bands of CNTs, inducing the depletion of the hole carriers. As a result, the hole depletion decreases the electrical conductivity of the *p*-type CNT transistors [21,22].

Moreover, the electrostatic gating effects can be induced by charged species adsorbed on CNTs. Therefore, target species can be distinguished by the sCNT transistors.

On the other hand, Schottky barrier modulation is a relevant mechanism to explain the sensing of floating electrode-based CNT sensors. The binding of target species to probes immobilized on the surfaces of metal floating electrodes can modulate the work function of the metal [22,23]. For example, the adsorption of positively charged species on or near the metal-CNT contact regions raises the metal work function Φ_M, resulting in the decrease of Schottky barrier height Φ_B (Figure 1.3(b)) [17]. For *p*-type sCNT transistors, Φ_B is an energy barrier formed at the metal-CNT contact region against the flow of hole carriers from the metal electrode to the sCNT [20]. Therefore, a Φ_B reduction increases the hole carrier transport from the electrode to the sCNT, inducing the conductance increase in the *p*-type sCNT transistors.

1.4. Fabrication procedure of sCNT transistors

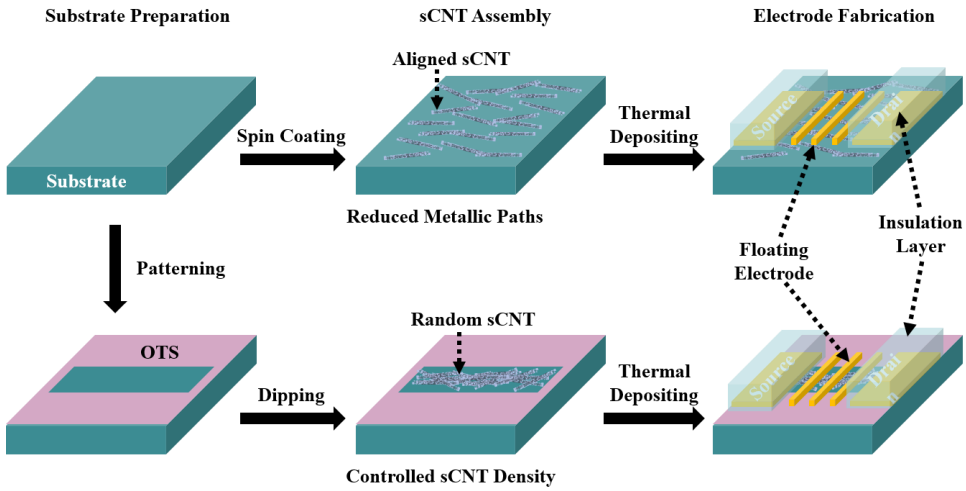

Figure 1.4. Schematic diagram showing the fabrication procedure of sCNT transistors.

In this dissertation, glass slides or silicon wafers were utilized as substrates to fabricate sCNT transistors. Figure 1.4 illustrates the fabrication procedure of sCNT transistors by two different sCNT assembly methods. Glass slides were soaked into a piranha solution (the 3:1 mixture of a concentrated sulfuric acid solution and a 30% wt. hydrogen peroxide solution) to remove organic residues on the surface before CNT assembly. CNT solutions were prepared by the dispersion of sCNTs in 1,2-dichlorobenzene via an ultrasonication. Then, CNTs were assembled on the substrates by a spin coating method or a dipping method. For the spin coating method, a CNTs suspension was spin coated on the substrate at 5000 rpm. Meanwhile, a self-assembled monolayer of octadecyltrichlorosilane with nonpolar terminal groups was adsorbed on the substrate to form channel patterns for the dipping method. To assemble CNTs on channels, the patterned substrate was immersed in the CNT solution for 10 s and rinsed with 1,2-dichlorobenzene. Subsequently, the source, drain, and floating electrodes (Pd/Au, 10 nm/30 nm) were fabricated by conventional photolithography

processes including a thermal evaporation deposition and a lift-off process. Lastly, source and drain electrodes were passivated by an aluminum oxide layer (Al_2O_3, 100 nm) or a photoresist layer (DNR) to eliminate leakage currents during electrical measurements in an aqueous environment.

1.5. Basic characteristics of sCNT transistors

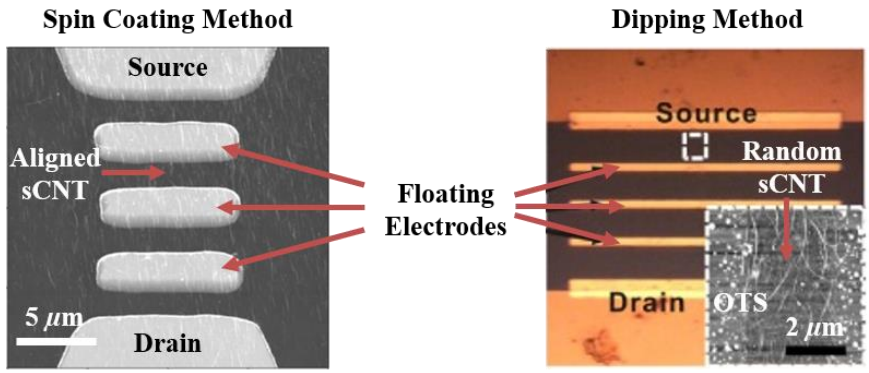

Figure 1.5. Topography image of sCNT transistors with three floating electrodes using two different CNT assembling methods.

Topography image of sCNT transistors taken by an atomic force microscopy (AFM) system (MFP-3D, Asylum Research) in a tapping mode shows the orientation of CNTs in junction areas of the transistors with three floating electrodes (Figure 1.5) [11,24]. Using the spin coating method, almost CNTs aligned along the channel direction. Previous works reported that the alignment of CNTs could improve the connectivity between electrodes and reduce lateral connections between current paths. Therefore, the formation of semiconducting paths was significantly increased, resulting in the enhancement of a device transconductance and a sensor sensitivity [25,26]. On the other hand, for the assembly of CNT by the dipping method, OTS patterns could increase the density of CNTs in a channel. The AFM image shows only a small portion of CNTs near channel boundaries was aligned along the channel direction, while most of them in the middle of the channel exhibited random orientations. The channel also exhibited well-defined boundaries without any crossing of CNTs, which indicates that the dipping method can be utilized for the highly selective assembly of purified sCNTs.

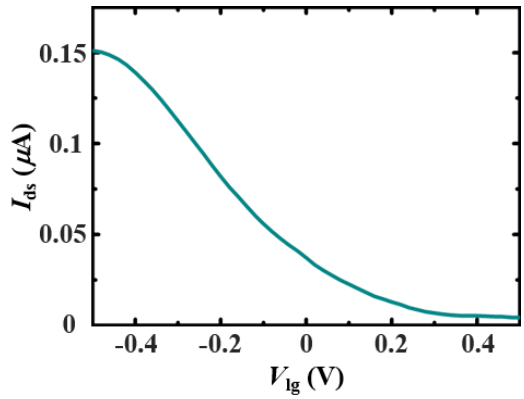

Figure 1.6. Liquid gating effect of a sCNT transistor measured in a buffer solution.

Figure 1.6 shows the gating effect curve of a sCNT transistor obtained by using an Ag/AgCl liquid gate electrode as a liquid gate in a buffer solution. A bias voltage between source and drain electrodes was maintained at 0.1 V, while a gate bias voltage (V_{lg}) was swept from -0.5 to 0.5 V. The source-drain current (I_{ds}) of the transistor was measured by a semiconductor characterization system (Keithley, 4200, USA). The curve shows a decreasing source-drain current with an increasing gate bias. It implies that our device exhibited *p*-type characteristics. In addition, the current decreased drastically by a small gate bias change, indicating the high sensitivity of our sCNT transistors.

1.6. References

[1] Watson, H. Biological membranes. *Essays Biochem*. **2015**, *59*, 43.

[2] Palani, K.; Kumaran, D.; Burley, S. K.; Swaminathan, S. Structure of a periplasmic glucose-binding protein from Thermotoga maritima. *Acta Crystallogr. F*. **2012**, *68*, 1460.

[3] Demarche, S.; Sugihara, K.; Zambelli, T.; Tiefenauer, L.; Voros, J. Techniques for recording reconstituted ion channels. *Analyst*. **2011**, *136*, 1077.

[4] Ogasawara, H.; Grzybowski, M.; Hosokawa, R.; Sato, Y.; Taki, M.; Yamaguchi, S. A far-red fluorescent probe based on a phospha-fluorescein scaffold for cytosolic calcium imaging. *Chem. Commun.* **2018**, *54*, 299.

[5] Sauve, R.; Diarra, A.; Chahine, M.; Simoneau, C.; Morier, N.; Roy, G. Ca^{2+} oscillations induced by histamine H1 receptor stimulation in HeLa cells: Fura-2 and patch clamp analysis. *Cell Calcium*. **1991**, *12*, 165.

[6] Szmacinski, H.; Toshchakov, V.; Piao, W.; Lakowicz, J. R. Imaging of Protein Secretion from a Single Cell Using Plasmonic Substrates. *Bionanoscience*. **2013**, *3*, 30.

[7] Lee, C.; Lee, J. W.; Seo, J. Y.; Hwang, S. W.; Im, J. P.; Kim, J. S. Lupeol inhibits LPS-induced NF-kappa B signaling in intestinal epithelial cells and macrophages, and attenuates acute and chronic murine colitis. *Life Sci.* **2016**, *146*, 100.

[8] Gao, F.; Cai, X.; Wang, X.; Gao, C.; Liu, S.; Gao, F.; Wang, Q. Highly sensitive and selective detection of dopamine in the presence of ascorbic acid at graphene oxide modified electrode. *Sensor. Actuator. B Chem.* **2013**, *186*, 380.

[9] Liu, Y.; Kwa, T.; Revzin, A. Simultaneous detection of cell-secreted TNF-alpha and IFN-gamma using micropatterned aptamer-modified electrodes. *Biomaterials*. **2012**, *33*, 7347.

[10] Negulyaev Yu, A.; Savokhina, G. A.; Vedernikova, E. A. Calcium-permeable channels in HeLa cells. *Gen. Physiol. Biophys.* **1993**, *12*, 19.

[11] Ta, V. T.; Park, J.; Park, E. J.; Hong, S. Reusable floating-electrode sensor for the quantitative electrophysiological monitoring of a nonadherent cell. *ACS Nano*. **2014**, *8*, 2206.

[12] Sudibya, H. G.; Ma, J.; Dong, X.; Ng, S.; Li, L. J.; Liu, X. W.; Chen, P. Interfacing glycosylated carbon-nanotube-network devices with living cells to detect dynamic secretion of biomolecules. *Angew. Chem. Int. Ed. Engl.* **2009**, *48*, 2723.

[13] Tsai, C. C.; Yang, C. C.; Shih, P. Y.; Wu, C. S.; Chen, C. D.; Pan, C. Y.; Chen, Y. T. Exocytosis of a single bovine adrenal chromaffin cell: the electrical and morphological studies. *J. Phys. Chem. B.* **2008**, *112*, 9165.

[14] Wang, C. W.; Pan, C. Y.; Wu, H. C.; Shih, P. Y.; Tsai, C. C.; Liao, K. T.; Lu, L. L.; Hsieh, W. H.; Chen, C. D.; Chen, Y. T. In situ detection of chromogranin a released from living neurons with a single-walled carbon-nanotube field-effect transistor. *Small*. **2007**, *3*, 1350.

[15] Tilmaciu, C. M.; Morris, M. C. Carbon nanotube biosensors. *Front. Chem.* **2015**, *3*, 59.

[16] Kim, B.; Lee, J.; Namgung, S.; Kim, J.; Park, J. Y.; Lee, M. S.; Hong, S. DNA sensors based on CNT-FET with floating electrodes. *Sensor. Actuator. B Chem.* **2012**, *169*, 182.

[17] Lee, M.; Jung, J. W.; Kim, D.; Ahn, Y. J.; Hong, S.; Kwon, H. W. Discrimination of Umami Tastants Using Floating Electrode-Based Bioelectronic Tongue Mimicking Insect Taste Systems. *ACS Nano*. **2015**, *9*, 11728.

[18] Son, M.; Kim, D.; Park, K. S.; Hong, S.; Park, T. H. Detection of aquaporin-4 antibody using aquaporin-4 extracellular loop-based

carbon nanotube biosensor for the diagnosis of neuromyelitis optica. *Biosens. Bioelectron.* **2016**, *78*, 87.

[19] Heller, I.; Janssens, A. M.; Mannik, J.; Minot, E. D.; Lemay, S. G.; Dekker, C. Identifying the mechanism of biosensing with carbon nanotube transistors. *Nano Lett.* **2008**, *8*, 591.

[20] Di Bartolomeo, A. Graphene Schottky diodes: An experimental review of the rectifying graphene/semiconductor heterojunction. *Phys. Rep.* **2016**, *606*, 1.

[21] Cui, Y.; Duan, X. F.; Hu, J. T.; Lieber, C. M. Doping and electrical transport in silicon nanowires. *J. Phys. Chem. B.* **2000**, *104*, 5213.

[22] Kim, S. N.; Rusling, J. F.; Papadimitrakopoulos, F. Carbon Nanotubes for Electronic and Electrochemical Detection of Biomolecules. *Adv. Mater.* **2007**, *19*, 3214.

[23] Chen, R. J.; Choi, H. C.; Bangsaruntip, S.; Yenilmez, E.; Tang, X.; Wang, Q.; Chang, Y. L.; Dai, H. An investigation of the mechanisms of electronic sensing of protein adsorption on carbon nanotube devices. *J. Am. Chem. Soc.* **2004**, *126*, 1563.

[24] Lee, J.; Lee, H.; Kim, T.; Jin, H. J.; Shin, J.; Shin, Y.; Park, S.; Khang, Y.; Hong, S. Floating electrode transistor based on purified semiconducting carbon nanotubes for high source-drain voltage operation. *Nanotechnology*. **2012**, *23*, 085204.

[25] Lee, M.; Lee, J.; Kim, T. H.; Lee, H.; Lee, B. Y.; Park, J.; Jhon, Y. M.; Seong, M. J.; Hong, S. 100 nm scale low-noise sensors based on aligned carbon nanotube networks: overcoming the fundamental limitation of network-based sensors. *Nanotechnology*. **2010**, *21*, 055504.

[26] Lee, M.; Noah, M.; Park, J.; Seong, M. J.; Kwon, Y. K.; Hong, S. "Textured" network devices: overcoming fundamental limitations of nanotube/nanowire network-based devices. *Small*. **2009**, *5*, 1642.

Chapter 2. Reusable sCNT transistors for the evaluation of antihistamine drugs via Ca^{2+} influx into HeLa cells

2.1. Introduction

Histamine, which acts as a neurotransmitter in central nervous systems, can influence many biological processes such as neuronal excitation and immune regulation via the activation of histamine receptors on cell plasma membranes [1-4]. One type of the histamine receptors is histamine type 1 receptor (H1R) which belongs to the family of G-protein-coupled receptors. The activation of H1Rs by histamine triggers many intracellular electrophysiological signaling pathways including the increase of intracellular calcium ions (Ca^{2+}) by the opening of Ca^{2+} channels in a cell plasma membrane [2,5,6]. In non-excitable cells such as HeLa cells, the stimulation of H1Rs embedded in the cell membrane generates the rise of cytosolic free Ca^{2+} concentrations [7]. By measuring the changes of Ca^{2+} concentrations as well as Ca^{2+} influx into cells, the electrophysiological effects of histamine and antihistamine drugs could be evaluated. In order to quantitatively monitor the Ca^{2+} influx into the cells, sensitive and reliable measurement techniques are required.

The effects of histamine and antihistamine drugs have been studied extensively using various methods such as fluorescence assays and electrophysiological techniques [8-10]. On the other hand, nanoscale devices have been developed to explore the electrophysiological activities of adherent cells with rather easy procedures [11-13]. However, nanoscale devices usually exhibited different characteristics from one device to another, which made it difficult to quantitatively analyze the data measured by nano-devices. Furthermore, the direct growth of cells on devices might affect the

characteristics of the nano-devices, resulting in a difficulty in comparing the data measured by different nano-devices.

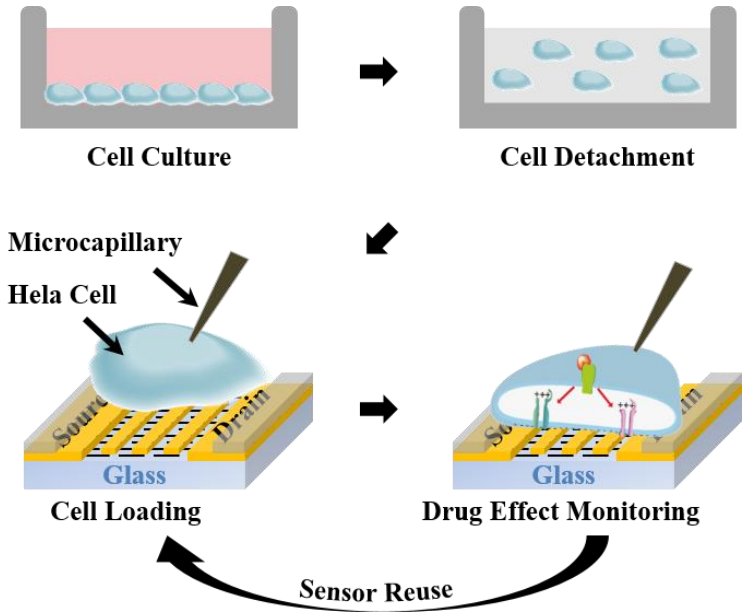

Figure 2.1. Schematic diagram depicting an experimental procedure for the monitoring of Ca^{2+} influx into a cell.

Herein, we report a method for the quantitative electrophysiological monitoring of the antihistamine drug effects on live cells using reusable sensors based on sCNT transistors (Figure 2.1). In this work, HeLa cells were first floated in a solution, and one of the cells was placed on the junction area of a reusable sensor via a microcapillary manipulation for the monitoring of its electrophysiological responses to histamine and antihistamine drugs. Significantly, for repeated measurements, the measured cell was replaced with a new cell on the same reusable sensor, enabling quantitative evaluation without being suffered from the device-to-device variation of device characteristics. The method was utilized to quantitatively monitor the electrophysiological responses of HeLa cells to histamine by evaluating the conductance changes of a reusable sensor. These conductance changes were attributed to Ca^{2+} influx through ion channels on a HeLa cell membrane due

to the activation of H1Rs by histamine. The pretreatments of HeLa cells with antihistamine drugs such as cetirizine or chlorphenamine reduced Ca^{2+} influx into the cells, which indicates that the activation of H1Rs was inhibited by antihistamine drugs [14]. Importantly, for each experimental set, we utilized only a single device to evaluate the activity of H1Rs in multiple HeLa cells, which allowed us to obtain statistically meaningful and quantitative results about the antihistamine drug effects without errors from device-to-device variations. Our work should provide a simple but powerful method for various biomedical applications such as drug screening and pharmaceutical studies at a single-cell-level.

2.2. Characteristics of reusable sensors

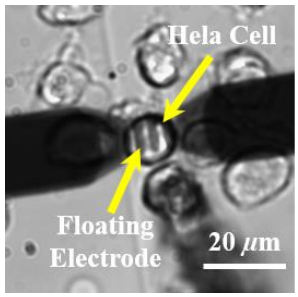

Figure 2.2. Microscopic image showing a Hela cell captured by using a microcapillary on a reusable sensor.

Figure 2.2 shows the optical image of a single HeLa cell placed on a CNT junction area using a microcapillary. Only the junction area including floating electrodes of the reusable sensor was exposed to a single HeLa cell during drug response experiments. It allows us to eliminate leakage currents and possible non-specific effects from other cells during sensing experiments in a liquid environment. Significantly, since HeLa cells were not directly cultured on device surfaces, they did not alter the characteristics of reusable sensors. Furthermore, the measured cell could be easily removed from sensor surfaces, and the used sensors could be reused for additional measurements with different cells, which allowed us to obtain statistically-meaningful results without suffering from possible errors due to device-to-device variations. Note that, unlike a patch clamp method, we do not need to form a hole or a high resistance seal on a cell membrane using a micropipette, and, thus, our method could be a convenient and non-invasive method. Furthermore, our method could quantitatively monitor electrophysiological signals at a single-cell-level, which would be a significant advantage for biomedical researches and applications.

2.3. Monitoring of histamine-induced Ca^{2+} influx into HeLa cells

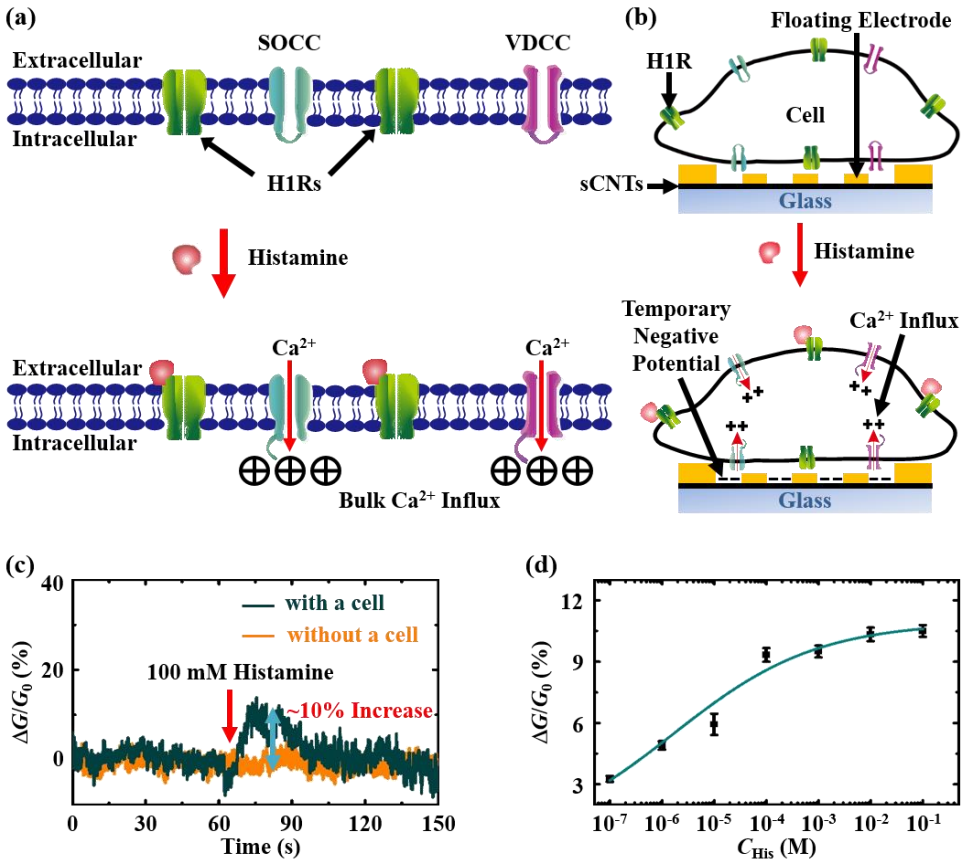

Figure 2.3. Quantitative electrophysiological monitoring of the effect of histamine drug on HeLa cells. (a) Schematic drawing sketching the mechanism of a histamine-stimulated Ca^{2+} influx into a cell via Ca^{2+} channels. (b) Schematic diagram showing the sensing mechanism of a reusable sensor for the monitoring of histamine-stimulated Ca^{2+} influx into a Hela cell. (c) Real-time responses of a reusable sensor with and without a Hela cell during the injection of 100 mM histamine. (d) Relative conductance changes of a single reusable sensor in response to Hela cells stimulated by histamine at various concentrations. Data are expressed as means ± SEM (standard error of the mean), (n = 3).

The changes of Ca^{2+} concentrations in cells could be mediated by two well-known mechanisms, namely Ca^{2+} releases from intracellular stores and Ca^{2+} influx through specialized channels on a plasma membrane [15,16]. Figure 2.3(a) depicts the mechanism of Ca^{2+} influx via store-operated calcium channels (SOCCs) and voltage-dependent calcium channels (VDCCs) opened by the histamine stimulation on H1Rs. HeLa cells are known to possess histamine receptors including H1Rs [9,14]. In a resting state, ion channels such as SOCCs and VDCCs on a cell membrane are closed. When histamine molecules interact with H1Rs, IP_3 molecules are generated as a second messenger in an intracellular signaling pathway. Subsequently, the activities of IP_3 induces Ca^{2+} release from intracellular stores which mediates Ca^{2+} influx through SOCCs referred to as capacitive Ca^{2+} entry. In turn, the further entry of Ca^{2+} is promoted through VDCCs which are opened by membrane depolarization [7,17,18].

Once Ca^{2+} flows into a cell through the opening of ion channels, a negative potential on the extracellular side of a plasma membrane increases (Figure 2.3(b)). Note that the electric currents of our reusable sensors increase with a negative gate bias (Figure 1.6). Thus, the stimulation of HeLa cells by histamine can cause the conductance increase of reusable sensors, which could be used to evaluate the interaction between ligands and receptors on a cell membrane. Figure 2.3(c) shows real-time relative conductance changes measured by a floating electrode-based reusable sensor with or without a HeLa cell during the injection of histamine. The relative conductance level of the reusable sensor with a HeLa cell increased by ~10% when a histamine solution was injected, while that of the reusable sensor without a cell exhibited no response. The conductance increase by the histamine injection could be attributed to the activity initiated by H1Rs in the HeLa cell. Once histamine molecules bound to H1Rs, Ca^{2+} flowed into the cell, which generated a temporary negative potential in a gap between the cell and the

CNT junction area of the reusable sensor (Figure 2.3(b)). Note that since our reusable sensor exhibited *p*-type characteristics, the increase of a negative potential would cause the increase of its conductance [19]. The increased conductance was recovered back to the original value after 50 s. This conductance recovery was probably due to the repolarization process of the cell and the charge balance of a bath solution. As reported previously, the influx of Ca^{2+}, which increased positive charges within a cell, was followed by the outflux of potassium ions (K^{+}) from the cell [2]. Moreover, cations in a bath solution could diffuse into the gap to neutralize excess negative charges. Both of these factors probably resulted in the conductance recovery of the reusable sensor after the response of the histamine injection. This data clearly indicates that our reusable sensors could detect the electrophysiological effects of histamine on HeLa cells. Significantly, since our method just measure the surrounding potential changes without damaging cells, it could be applied for the study of the electrophysiological responses of various cell lines in a non-invasive manner.

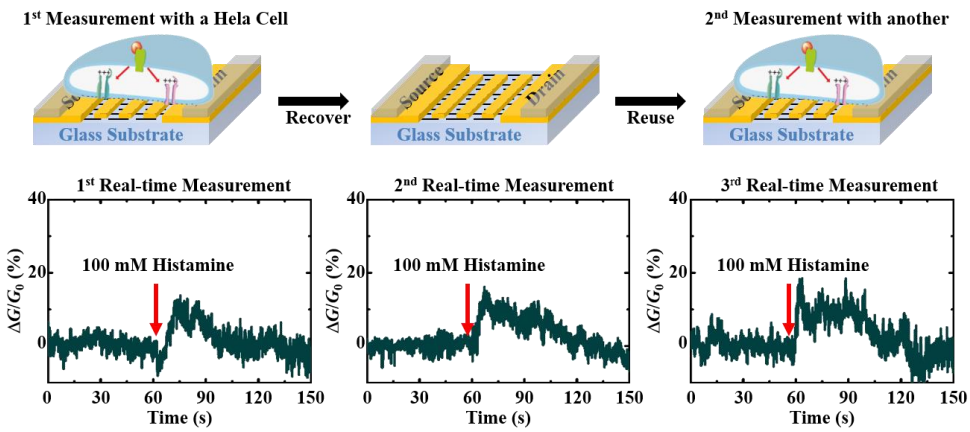

Figure 2.4. Repeated measurements for the responses of a single reusable sensor to multiple Hela cells during the injection of 100 mM histamine.

To confirm the repeatability of our reusable sensor, we carried out measurements three times for each concentration of histamine using the same

reusable sensor (Figure 2.4). Note that, even after twenty-one measurements, the responses of the reusable sensor still remained similar to the initial measurement, indicating our sensors can be repeatedly utilized for the electrophysiological monitoring of multiple cells.

The responses of a HeLa cell to histamine could be quantified by the relative conductance changes of our reusable sensor. Figure 2.3(d) shows the conductance responses of a reusable sensor by the stimulation of different concentration histamine solutions in the range from 100 nM to 100 mM. The dose-response curve was fitted by a Hill equation written as [20]

$$\Delta G/G_0 = \Delta G/G_{0\max} \frac{C_{\mathrm{His}}^n}{(EC_{50})^n + C_{\mathrm{His}}^n}$$

Here, $\Delta G/G_0$ and $\Delta G/G_{0\max}$ are a relative conductance change and the maximum value of relative conductance changes, respectively. C_{His} and EC_{50} are the concentration of histamine in a solution and the concentration of histamine giving a half-maximal relative conductance change, respectively. n is a Hill coefficient. In case of drug screening experiments, the potency of specific drugs can be represented by the values of pEC_{50} which is defined as $-\log_{10}(EC_{50})$. The fitting analysis on our data shows that the estimated value of pEC_{50} by histamine stimulation was 5.78 ± 0.23, which was similar to a previously-reported value measured by a fluorescent method [8]. Also, note that when the concentrations of histamine solutions were larger than 10 μM, the cell responses saturated and have similar values for different concentration histamine solutions, which is consistent with previous works [8,20,21]. Moreover, a such statistically-meaningful quantitative measurement was made possible because this method allows us to perform repeat measurements for multiple cells using a single reusable sensor device and thus to minimize possible errors from device-to-device variations of its characteristics.

2.4. Effect monitoring of antihistamine drugs on histamine-induced Ca^{2+} influx

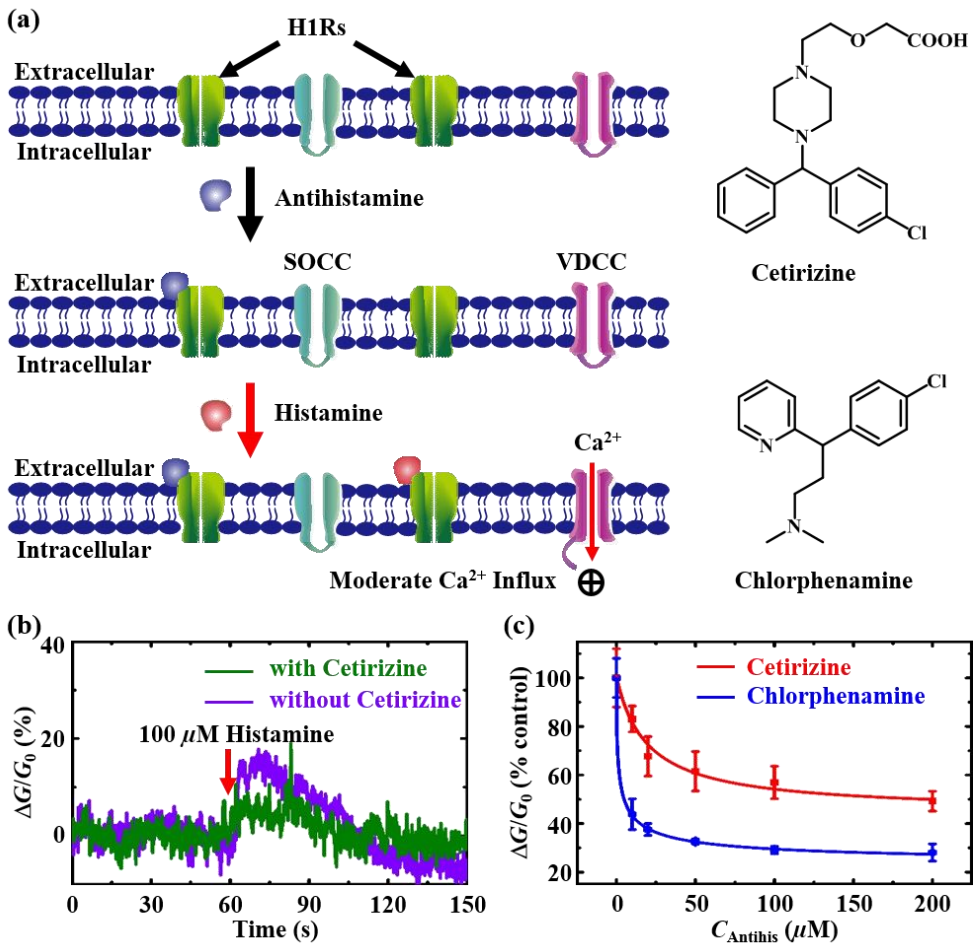

Figure 2.5. Quantitative electrophysiological monitoring of antihistamine drug effects using reusable sensors. (a) Schematic diagram of the effect mechanism of antihistamine drugs on histamine-stimulated Ca^{2+} influx into a Hela cell and chemical structures of them. (b) Real-time electrophysiological responses of cetirizine pretreated and non-pretreated HeLa cells to the injection of 100 μM histamine. (c) Dose dependent responses of reusable sensors to Hela cells pretreated with antihistamine drugs at various

concentrations during the injection of 100 μM histamine. Data are expressed as means ± SEM, (n = 3).

Figure 2.5(a) describes the mechanism of antihistamine drug effect on Ca^{2+} influx into a HeLa cell. In this work, we evaluated the effects of cetirizine and chlorphenamine as antihistamine drugs which were known as inverse agonists. Once inverse agonists bind with H1Rs, the H1Rs are converted to inactive forms, and the receptor activity of cells is down-regulated [14]. Thus, the activation of H1Rs by histamine is degraded, resulting in the decrease of Ca^{2+} influx through SOCCs into the cells. In turn, Ca^{2+} influx via the opening of VDCCs should be decreased due to the reduced membrane depolarization. Thus, the quantitative effects of antihistamine drugs to HeLa cells can be evaluated by monitoring the membrane potential change caused by the Ca^{2+} influx into the cells.

Figure 2.5(b) shows the real-time electrophysiological responses of HeLa cells pretreated with or without cetirizine, one of the antihistamine drugs. To study the effect of cetirizine, HeLa cells were incubated with a Ca^{2+}-free bath solution including 50 μM cetirizine for 15 min before the cells were transferred and assembled on a reusable sensor. To trigger Ca^{2+} influx into cells, a bath solution with histamine was injected so that the final concentration of histamine was 100 μM. The relative conductance change of the reusable sensor with the HeLa cell pretreated with cetirizine was ~5%, which was significantly smaller than that of the reusable sensor with a non-pretreated HeLa cell (~13%). This result indicates that cetirizine worked as an antihistamine drug on the HeLa cells assembled on the reusable sensor, and our method can be utilized to measure the effect of antihistamine drugs in real time.

We could also quantitatively monitor the electrophysiological effects of different antihistamine drugs with various concentrations (Figure 2.5(c)). Here, HeLa cells were incubated with bath solutions including cetirizine or

chlorphenamine with various concentrations ranging from 10 to 200 μM. Then, the response of individual HeLa cells by the injection of 100 μM histamine was measured using a single reusable sensor. For a reliable statistical analysis, we repeated measurements three times for each antihistamine drug concentration using the same reusable sensor. Dose-response curves showed the drastic decrease of the relative conductance changes of a reusable sensor for HeLa cells pretreated with chlorphenamine. Importantly, the relative conductance changes of a reusable sensor for HeLa cells pretreated with cetirizine were smaller than those with chlorphenamine. The result is also consistent with previous reports showing that chlorphenamine was a stronger inverse agonist than cetirizine [14,22]. To quantitatively estimate the effect of antihistamine drugs, the results were analyzed by a Hill equation for inhibitors like

$$\Delta G/G_0 = \Delta G/G_{0\min} + (\Delta G/G_{0\max} - \Delta G/G_{0\min})\frac{(IC_{50})^n}{(IC_{50})^n + C_{\text{Antihis}}^n}$$

Here, $\Delta G/G_{0\min}$ is the minimum value of relative conductance changes. C_{Antihis} and IC_{50} are the concentration of an antihistamine drug in a solution and that of an antihistamine drug giving a half-maximal relative conductance change, respectively. Antihistamine drugs are inhibition drugs whose role is blocking the binding of histamine to receptors. In this case, the potency of such drugs can be evaluated by a pIC_{50} value which is defined as -$\log_{10}(IC_{50})$ and representing an inhibition efficiency rather than a binding efficiency. By fitting the data, pIC_{50} values for cetirizine and chlorphenamine were directly calculated from dose-response curves to be 4.70 and 5.77, respectively. These pIC_{50} values quantitatively indicate that the measured potency of chlorphenamine was higher than that of cetirizine as reported previously [22]. Significantly, previous works show that chlorphenamine inhibited the activity of H1Rs with pIC_{50} values in the range of 3.86 - 6.28, which is consistent with our measurement results [23-25]. This result supports the validity of our

method. Furthermore, the measured response data in Figure 2.5(c) can be utilized to estimate the quantity of H1Rs which were still active with antihistamine drugs. For example, the HeLa cells pretreated with 10 μM chlorphenamine exhibited a relative conductance change of ~40% compared with the response of non-pretreated cells. It implies that ~60% of H1Rs on a cell membrane shifted to inactive forms by chlorphenamine, which was consistent with previous results measured by conventional methods [14]. To fully appreciate our method, the Cheng-Prusoff equation was used to estimate inhibitor constants, K_i, which are indicators for the efficiency of drugs [26].

$$K_i = \frac{IC_{50}}{1 + \frac{C_{His}}{EC_{50}}}$$

pK_i values, defined as -$\log_{10}(K_i)$, for cetirizine and chlorphenamine were calculated from the Cheng-Prusoff equation to be 6.49 and 7.56, respectively. These results clearly show that our method can be utilized to quantitatively evaluate the effect of antihistamine drugs. Considering that the statistically-meaningful quantitative measurement of drug effects using high-performance nanoscale devices have been extremely difficult due to rather large device-to-device variations of its characteristics, our strategy can be a significant breakthrough in the various applications of nanoscale devices such as drug screenings and electrophysiological study of cell activities.

2.5. Summary

In summary, we report a strategy using a single reusable sensor device to quantitatively monitor the electrophysiological responses of multiple individual cells to histamine and antihistamine drugs. Here, we could repeatedly measure the real-time response of HeLa cells to histamine drugs quantitatively using the same reusable sensor device. Results have showed that our method enables the statistically-meaningful quantitative evaluations without suffering from the errors by the device-to-device variations of sensor characteristics. Using this method, we demonstrated the quantitative evaluation of the effect of antihistamine drugs such as cetirizine and chlorphenamine and found that chlorphenamine had a better efficacy than cetirizine as reported previously [22]. Since our strategy takes an advantage of high-performance nanoscale devices while still enabling the statistically-meaningful evaluations, it can be a powerful tool for various applications such as drug screening and therapeutic monitoring.

2.6. References

[1] Akdis, C. A.; Blaser, K. Histamine in the immune regulation of allergic inflammation. *J. Allergy Clin. Immunol.* **2003**, *112*, 15.

[2] Benarroch, E. E. Histamine in the CNS: multiple functions and potential neurologic implications. *Neurology*. **2010**, *75*, 1472.

[3] MacGlashan, D., Jr. Histamine: A mediator of inflammation. *J. Allergy Clin. Immunol.* **2003**, *112*, S53.

[4] Schneider, E.; Rolli-Derkinderen, M.; Arock, M.; Dy, M. Trends in histamine research: new functions during immune responses and hematopoiesis. *Trends Immunol.* **2002**, *23*, 255.

[5] Jutel, M.; Akdis, M.; Akdis, C. A. Histamine, histamine receptors and their role in immune pathology. *Clin. Exp. Allergy*. **2009**, *39*, 1786.

[6] Molina-Hernandez, A.; Diaz, N. F.; Arias-Montano, J. A. Histamine in brain development. *J. Neurochem.* **2012**, *122*, 872.

[7] Barajas, M.; Andrade, A.; Hernandez-Hernandez, O.; Felix, R.; Arias-Montano, J. A. Histamine-induced Ca^{2+} entry in human astrocytoma U373 MG cells: evidence for involvement of store-operated channels. *J. Neurosci. Res.* **2008**, *86*, 3456.

[8] Bootman, M. D.; Berridge, M. J.; Taylor, C. W. All-or-nothing Ca^{2+} mobilization from the intracellular stores of single histamine-stimulated HeLa cells. *J. Physiol.* **1992**, *450*, 163.

[9] Sauve, R.; Diarra, A.; Chahine, M.; Simoneau, C.; Morier, N.; Roy, G. Ca^{2+} oscillations induced by histamine H1 receptor stimulation in HeLa cells: Fura-2 and patch clamp analysis. *Cell Calcium*. **1991**, *12*, 165.

[10] Negulyaev Yu, A.; Savokhina, G. A.; Vedernikova, E. A. Calcium-permeable channels in HeLa cells. *Gen. Physiol. Biophys.* **1993**, *12*, 19.

[11] Cheng, J.; Wu, L.; Du, X. W.; Jin, Q. H.; Zhao, J. L.; Xu, Y. S. Flexible Solution-Gated Graphene Field Effect Transistor for

Electrophysiological Recording. *J. Microelectromech. Syst.* **2014**, *23*, 1311.

[12] Li, B. R.; Hsieh, Y. J.; Chen, Y. X.; Chung, Y. T.; Pan, C. Y.; Chen, Y. T. An ultrasensitive nanowire-transistor biosensor for detecting dopamine release from living PC12 cells under hypoxic stimulation. *J. Am. Chem. Soc.* **2013**, *135*, 16034.

[13] Spanu, A.; Lai, S.; Cosseddu, P.; Tedesco, M.; Martinoia, S.; Bonfiglio, A. An organic transistor-based system for reference-less electrophysiological monitoring of excitable cells. *Sci. Rep.* **2015**, *5*, 8807.

[14] Mizuguchi, H.; Ono, S.; Hattori, M.; Sasaki, Y.; Fukui, H. Usefulness of HeLa cells to evaluate inverse agonistic activity of antihistamines. *Int. Immunopharmacol.* **2013**, *15*, 539.

[15] Berridge, M. J. Elementary and global aspects of calcium signalling. *J. Physiol.* **1997**, *499*, 291.

[16] Streb, H.; Irvine, R. F.; Berridge, M. J.; Schulz, I. Release of Ca^{2+} from a nonmitochondrial intracellular store in pancreatic acinar cells by inositol-1,4,5-trisphosphate. *Nature*. **1983**, *306*, 67.

[17] Dai, Y.; Zhang, J. H. Manipulation of chloride flux affects histamine-induced contraction in rabbit basilar artery. *Am. J. Physiol. Heart Circ. Physiol.* **2002**, *282*, H1427.

[18] Nemeth, K.; Kurucz, I. Suppression of Ca^{2+} influx by unfractionated heparin in non-excitable intact cells via multiple mechanisms. *Biochem. Pharmacol.* **2005**, *69*, 929.

[19] Ta, V. T.; Park, J.; Park, E. J.; Hong, S. Reusable floating-electrode sensor for the quantitative electrophysiological monitoring of a nonadherent cell. *ACS Nano*. **2014**, *8*, 2206.

[20] Bristow, D. R.; Zamani, M. R. Desensitization of histamine H1 receptor-mediated inositol phosphate production in HeLa cells. *Br. J. Pharmacol.* **1993**, *109*, 353.

[21] Volpi, M.; Berlin, R. D. Intracellular Elevations of Free Calcium Induced by Activation of Histamine-H1 Receptors in Interphase and Mitotic Hela-Cells - Hormone Signal Transduction Is Altered during Mitosis. *J. Cell Biol.* **1988**, *107*, 2533.

[22] Christophe, B.; Carlier, B.; Gillard, M.; Chatelain, P.; Peck, M.; Massingham, R. Histamine H1 receptor antagonism by cetirizine in isolated guinea pig tissues: influence of receptor reserve and dissociation kinetics. *Eur. J. Pharmacol.* **2003**, *470*, 87.

[23] Markwardt, K. L.; Magnino, P. E.; Pang, I. H. Effect of histamine on phosphoinositide turnover and intracellular calcium in human ciliary muscle cells. *Exp. Eye Res.* **1996**, *62*, 511.

[24] Sakuta, H. Inhibition by histamine H1 receptor antagonists of endogenous glibenclamide-sensitive K^+ channels in follicle-enclosed Xenopus oocytes. *Eur. J. Pharmacol.* **1994**, *266*, 99.

[25] Salata, J. J.; Jurkiewicz, N. K.; Wallace, A. A.; Stupienski, R. F., 3rd; Guinosso, P. J., Jr.; Lynch, J. J., Jr. Cardiac electrophysiological actions of the histamine H1-receptor antagonists astemizole and terfenadine compared with chlorpheniramine and pyrilamine. *Circ. Res.* **1995**, *76*, 110.

[26] Lazareno, S.; Birdsall, N. J. M. Estimation of Competitive Antagonist Affinity from Functional Inhibition Curves Using the Gaddum, Schild and Cheng-Prusoff Equations. *Br. J. Pharmacol.* **1993**, *109*, 1110.

Chapter 3. Nafion-radical films on sCNT transistors for the evaluation of antipsychotic drugs via dopamine release from PC12 cells

3.1. Introduction

Dopamine is one of the important neurotransmitters, which regulates a wide variety of functions in the central nervous system. Dopamine dysfunctions in the nervous system are concerned with various neurological symptoms such as Parkinson's disease and schizophrenia [1,2]. It has been reported that the concentration changes of potassium ions (K^+) in the brain may induce neurological disorders including the release of neurotransmitters as dopamine [3,4]. Therefore, the real-time monitoring of the K^+-evoked dopamine release from neural cells should be important for the understanding of dopaminergic dysfunctions. Moreover, the primary therapy of schizophrenia is based on the regulation of dopaminergic functions by antipsychotic drugs. Previously, it was reported that antipsychotic drugs inhibited dopamine receptor activities and reduced K^+-evoked dopamine release [2,5]. Thus, one method to monitor the efficacy of antipsychotic drugs can be the monitoring of the dopamine release from drug-pretreated cells under K^+-stimulation.

Field-effect transistor (FET) devices have shown distinct advantages, and they have been extensively used to detect dopamine in various environments [6-9]. However, they were not utilized to evaluate the efficacy of actual antipsychotic drugs as well as real-time cellular measurements. Herein, we report a Nafion-radical hybrid film on a floating electrode-based sCNT sensor to monitor the effects of an antipsychotic drug, pimozide, on the dopamine release from living cells (Figure 3.1).

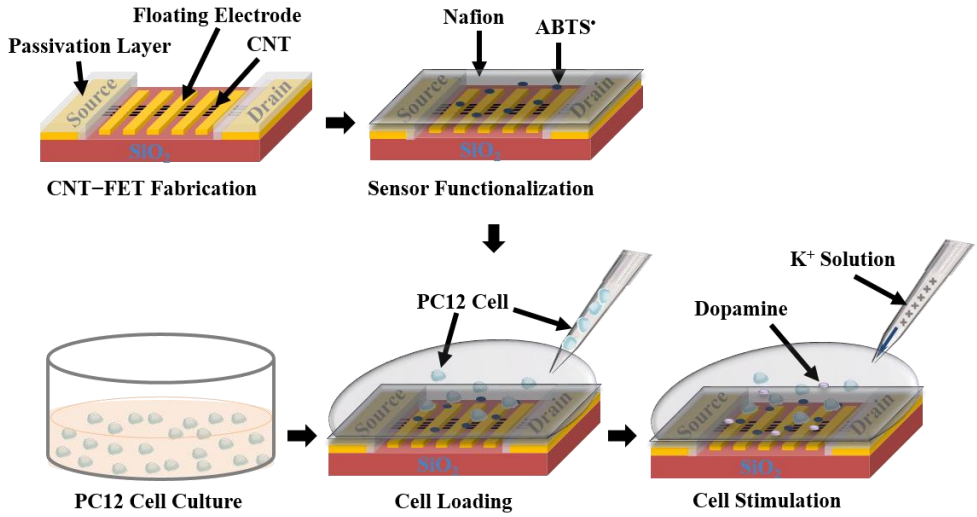

Figure 3.1. Schematic diagram depicting preparatory processes for the detection of dopamine released from living PC12 cells by using an NRC sensor.

In this work, a floating electrode-based CNT-FET device was coated by a Nafion film containing 2,2'-azino-bis(3-ethylbenzothiazoline-6-sulfonic acid) (ABTS•) radicals to build a selective biosensor (NRC sensor) for the detection of dopamine. In aqueous solution, ABTS• radicals can selectively react with dopamine, which was detected by underlying sensors for selective sensing. Negatively charged Nafion films not only acts as catalytic layers to positively charged dopamine molecules but also as a matrix holding ABTS• radicals to enhance the sensitivity of NRC sensors to dopamine. This sensor can selectively monitor the variation of dopamine concentrations down to a 10 nM level and distinguish dopamine from other neurotransmitters. We demonstrated the real-time monitoring of K^+-evoked dopamine release from PC12 cells using our sensors. Significantly, the sensors were utilized to evaluate the effects of pimozide on the dopamine release of K^+-stimulated PC12 cells. This is a selective and sensitive sensor, which can be utilized for versatile biological and medical applications.

3.2. Characteristics of NRC sensors

To build NRC sensors, a Nafion solution (0.5% in ethanol) containing 1.4 mM ABTS and 0.49 mM $K_2S_2O_8$ was mixed in an ultrasonic bath for 30 min to form a coating solution. Afterward, 2 μL of the coating solution containing ABTS$^{\bullet}$ radicals was directly dropped on a floating electrodes-based CNT-FET device. Then, the device was dried in a nitrogen atmosphere at room temperature to form a stable and thin film upon the device.

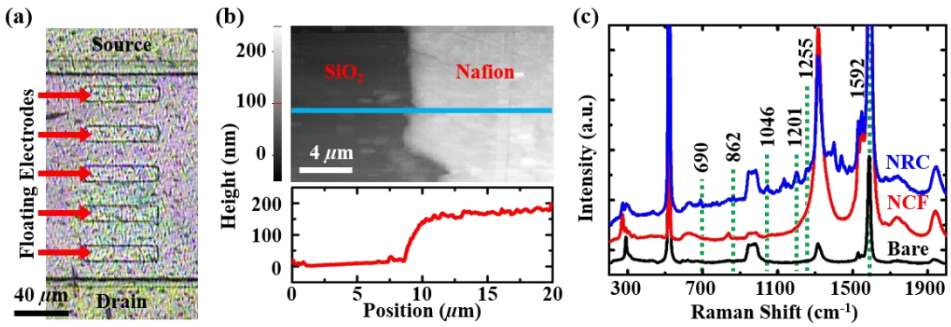

Figure 3.2. Characterization of a Nafion-radical hybrid film on a floating electrode-based CNT sensor. (a) Optical image of an NRC sensor. (b) AFM topography image with a height profile of a nafion-radical hybrid film on an NRC sensor. (c) Raman spectra of the CNT regions of an NRC sensor (marked by "NRC") and two different CNT-FET devices: a floating electrode-based CNT-FET device coated with a Nafion layer (marked by "NCF") and a bare floating electrode-based CNT-FET device (marked "Bare").

The quality of an NRC sensor was checked by imaging the surface structure of the sensor. Figure 3.2(a) shows the optical image of an NRC sensor including five floating electrodes and the topography image of a sensor surface. The optical image was obtained by using an optical microscope (XY-MRT, Sunny) equipped with a charge-coupled device (CCD) camera (SDC-415S, Samsung). The image shows well-defined electrodes with the 10 μm × 60 μm dimension for each floating electrode. Furthermore, the topography image of an NRC sensor taken by an AFM system in tapping mode with a

scan rate of 0.3 Hz shows a uniform Nafion layer on the NRC sensor (Figure 3.2(b)). The thickness of the Nafion film could be estimated as ~200 nm using the AFM topography image on the boundary of the film.

To confirm the functionalization of an NRC sensor by ABTS$^{\bullet}$ radicals, we performed the Raman scattering spectroscopy analysis on the devices with or without ABTS$^{\bullet}$ radicals. Figure 3.2(c) shows the Raman spectra of an NRC sensor, a floating electrode-based CNT-FET device coated with a pure Nafion layer without ABTS$^{\bullet}$ radicals (NCF sensor), and a bare CNT-FET device with floating electrodes. Raman spectra were measured at CNT channel areas by using a Raman spectroscope (XperRam 200, Nanobase) in a single mode. The Raman spectrum (black line) of CNTs on a bare device exhibits a rather large G-band peak (1588 cm^{-1}) as well as a much smaller D-band peak (1314 cm^{-1}), indicating the small number of defects in the used sCNTs [10,11]. These results support the high quality of sCNT channels in our devices. The Raman spectra of the NRC sensor exhibit vibration bands at characteristic wavenumbers such as 690, 862, 1046, 1201, 1255, and 1592 cm^{-1}, which can be associated with ABTS$^{\bullet}$ radicals as reported previously [12,13]. It indicates the presence of ABTS$^{\bullet}$ radicals in the Nafion layer on the NRC sensor. This result clearly shows that our device was successfully functionalized with a Nafion-radical hybrid film.

3.3. Discrimination of dopamine by NRC sensors

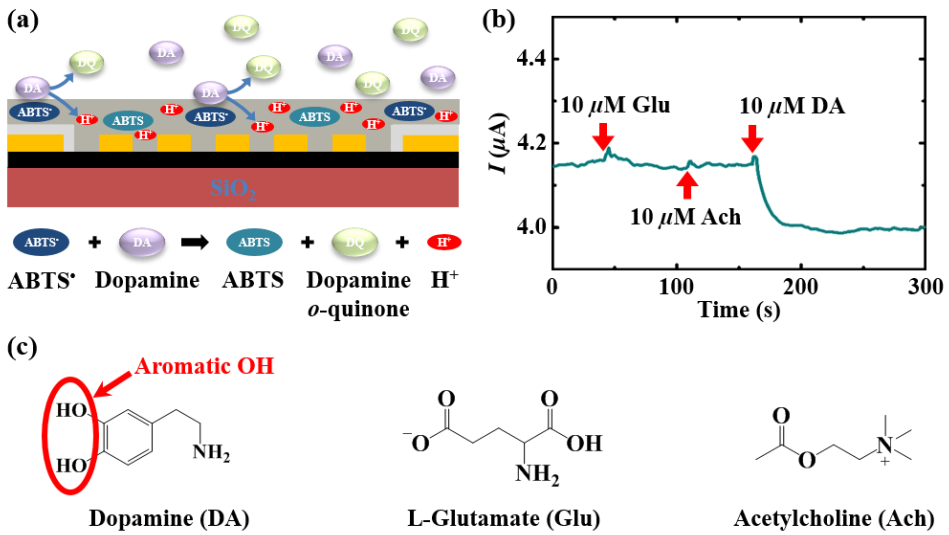

Figure 3.3. Responses of an NRC sensor to the presence of neurotransmitter solutions. (a) Schematic diagram showing the sensing mechanism of NRC sensors to dopamine. (b) Real-time responses of an NRC sensor to different neurotransmitters such as L-glutamate (Glu), acetylcholine (Ach), and dopamine (DA). (c) Chemical structures of the neurotransmitters.

Figure 3.3(a) depicts a schematic diagram showing the sensing mechanism of an NRC sensor for dopamine molecules. Once dopamine molecules approach the surface of an NRC sensor, redox reactions between dopamine molecules and ABTS• radicals occur [14-16]. These redox reactions generate H^+, which can interact with the sulfonate groups of Nafion, resulting in the increase of positive potentials in a Nafion film on the NRC sensor. Here, Nafion not only acts as an ion binder and a signal transporter, but also plays a role as an insulator to prevent the effects of an ambient environment on the sensor. Note that as CNT channels in our sensors exhibited *p*-type characteristics, the increase of positive potentials would cause the decrease of their conductance (Figure 1.6). Thus, once a dopamine

solution is added on an NRC sensor, the increased positive potential in the Nafion film upon the device causes the decreased electrical conductance.

To investigate the selectivity of our NRC sensor, we measured electrical currents through an NRC sensor during the additions of other neurotransmitters such as glutamate and acetylcholine, which can be released with dopamine from stimulated cells [17]. Figure 3.3(b) shows the electrical current changes in an NRC sensor during the additions of various neurotransmitters. The graph indicates that only the addition of dopamine caused an electrical current decrease, whereas the additions of glutamate and acetylcholine did not affect the electrical current in the NRC sensor. These results show that our NRC sensor could be used to selectively detect dopamine even in a mixed solution. Note that the responses of NRC sensors come from the interactions between $ABTS^{\bullet}$ radicals and aromatic hydroxyl (OH) groups. Therefore, our sensors can be applied to detect a broad range of biomolecules with aromatic OH groups such as dopamine, uric acid, and ascorbic acid. In our work, the NRC sensors were used to monitor dopamine released from cells stimulated by K^+. In this case, K^+-stimulated cells are reported to release neurotransmitters such as dopamine, glutamate, and acetylcholine, and dopamine is the only chemical substance with aromatic OH groups (Figure 3.3(c)) [4,17-19]. Thus, we performed the selective sensing experiments with other neurotransmitters, showing that our method can be used to selectively detect dopamine out of all neurotransmitters released from K^+-stimulated cells.

Figure 3.4(a) shows the real-time changes of electrical currents in an NRC sensor during the additions of dopamine solutions at various concentrations in the range of 10 nM to 100 μM. The graph shows a sharp decrease in the source-drain current of the NRC sensor after the addition of a dopamine solution, and then the electrical current gradually stabilizes. However, there were no significant changes in an electrical current through a

bare floating electrode-based CNT-FET device during the additions of dopamine solutions (Figure 3.4(b)). Note that the NRC sensor exhibited current changes much larger than noise amplitudes even at 10 nM. These results indicate that our method can discriminate dopamine at various concentrations with the detection limit of 10 nM, which is lower than most of previous sensors (Table 3.1).

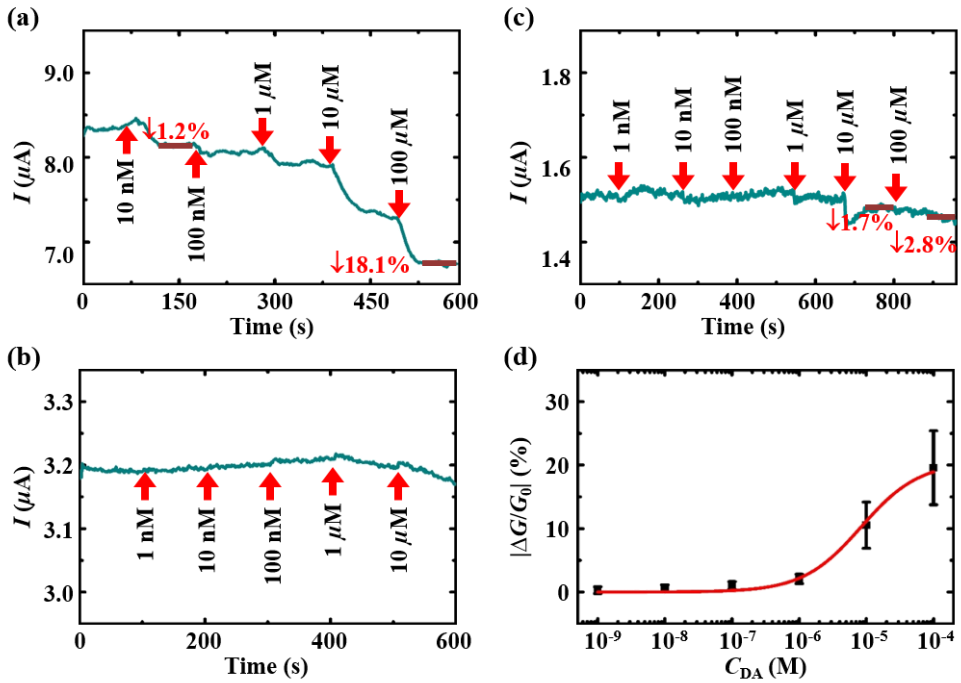

Figure 3.4. Responses of three different sCNT sensors to the presence of dopamine solutions. Real-time electrical current measurements of an NRC sensor (a), an NCF sensor (b) and a bare sensor (c) during the additions of dopamine solutions with different concentrations ranging from 1 nM to 100 μM. (d) Dose-dependent responses of NRC sensors to various concentrations of dopamine. Data are expressed as means ± SEM, (n = 5).

As a control experiment, we measured the response of an NCF sensor to dopamine (Figure 3.4(c)). The results show negligible current changes of less than 3% by the dopamine with the concentrations up to 100 μM, which is much smaller than the signals by our NRC sensors with ABTS$^{\bullet}$ radicals. The

response of the NCF sensor may be attributed to the electrostatic interactions between dopamine molecules and the Nafion film, which may also cause unexpected effects on the responses of NRC sensors to dopamine [6,14,20]. However, the control experiment results show that these effects are not significant for dopamine concentrations up to 100 μM. It also should be mentioned that the response time of our sensor was ~25 s, which was rather fast compared with previous dopamine sensors (Table 3.1). Previous works showed that the diffusion time of H^+ in a Nafion film depended on the film thickness, which may delay sensor responses [21]. However, in our case, the response time of the sensor was rather fast compared with previous works and enough for practical applications, indicating that the time delay by the diffusion in the Nafion film was not a significant problem in our sensors. Moreover, the quick responses of the NRC sensor imply that our sensors can be used for real-time monitoring applications.

Table 3.1. Detection limit and response time of NRC sensors to dopamine detection comparing with previous methods.

Method	Detection Limit	Response Time	Reference
Electrochemistry	5 µM	20 - 40 sec	[18]
Graphene-FET	1 nM	100 sec	[6]
CNT-FET	1 µM	No data	[7]
HPLC	163nM	8 min	[22]
Electrochemistry	1 µM	No data	[14]
Electrochemistry	50 µM	100 sec	[20]
CNT-FET	10 nM	25 sec	This work

Figure 3.4(d) shows the normalized conductance changes of our sensors exposed to dopamine solutions with difference concentrations (C_{DA}). The dose-response curve indicated a wide dynamic range (1 nM to 100 μM) where

our sensors can be used for monitoring dopamine levels. Sensing measurements were repeatedly performed five time with different NRC sensors to confirm the reliability. Significantly, the equilibrium constant K_{eq} of redox reactions between ABTS$^{\bullet}$ radicals and dopamine could be estimated by fitting data with the Langmuir thermal equation given by [23,24]

$$\left|\Delta G/G_0\right| = \left|\Delta G/G_0\right|_{max} \frac{C_{DA}}{1/K_{eq} + C_{DA}}$$

where $|\Delta G/G_0|$ and $|\Delta G/G_0|_{max}$ represent the absolute value of a relative conductance change and its maximum absolute value. On the basis of this model, the value of K_{eq} was estimated as $10^{5.08\pm0.21}$. Previous reports showed that the formal standard redox potential ($E^{0'}$) values of ABTS and dopamine are 0.47 V (vs Ag/AgCl) and 0.75 V (vs standard hydrogen electrode (SHE)), respectively [15,16].

2×	$ABTS^{\bullet} + e \rightarrow ABTS$	$E^{0'}_{ABTS^{\bullet}/ABTS} = 0.47$ V
1×	$DA \rightarrow DQ + 2H^+ + 2e$	$E^{0'}_{DQ,\,H^+(1M)/DA} = 0.75$ V
	$2ABTS^{\bullet} + DA \rightarrow 2ABTS + DQ + 2H^+$	$\Delta E^{0'}$

The relation between the standard electrode potential $\Delta E^{0'}$ and the equilibrium constant K_{eq} of the redox reaction could be written by

$$\Delta E^{0'} = E^{0'}_{ABTS^{\bullet}/ABTS} - \left(E^{0'}_{DQ,\,H^+(1M)/DA} - 0.05916 \times pH \right) = \frac{0.05916}{n} \times \log K_{eq}$$

At $pH = 7.4$ and the number of transferred electrons $n = 2$, the equilibrium constant K_{eq} of the redox reaction calculated based on these $E^{0'}$ values is $10^{5.33}$, which is similar to the value estimated by NRC sensors.

3.4. Real-time monitoring of K^+-evoked dopamine release from PC12 cells using NRC sensors

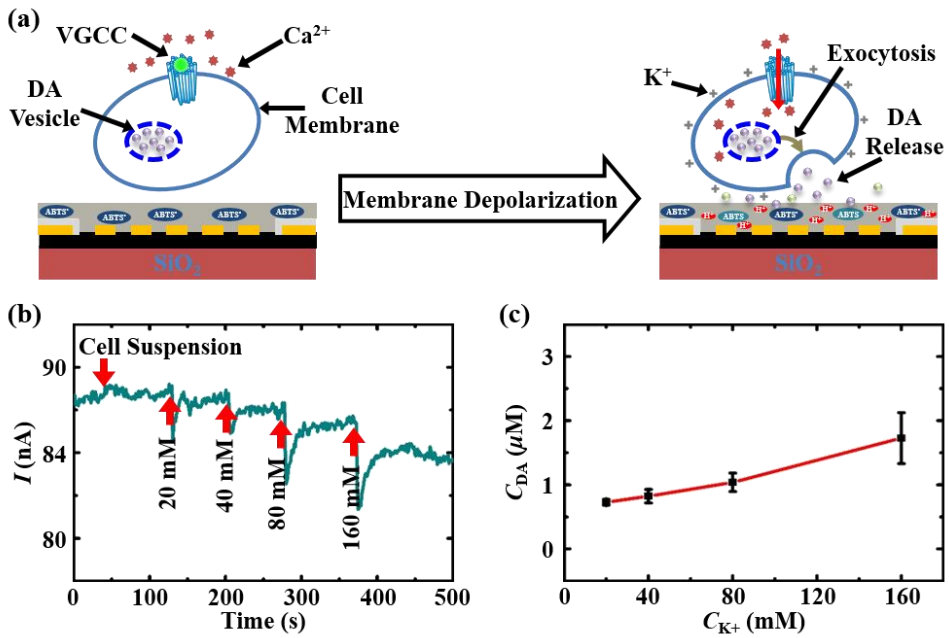

Figure 3.5. Quantitative monitoring of dopamine release from living PC12 cells under the stimulation of K^+ solutions. (a) Schematic diagram showing the mechanism of dopamine release from PC12 cells stimulated by a high-concentrated K^+ solution and the real-time monitoring of the dopamine release by an NRC sensor. (b) Real-time current changes measured by an NRC sensor during the additions of a cell suspension solution and concentrated K^+ solutions at various concentrations. (c) Dose-response curve for the stimulation of different K^+ solutions on dopamine release from PC12 cells. Data are expressed as means ± SEM, (n = 5).

As the mechanism of dopamine release from PC12 cells is similar to that from neurons, PC12 cells have been extensively used as a dopaminergic model for neurobiological studies [5,25]. Figure 3.5(a) depicts the mechanism for the responses of an NRC sensor to dopamine molecules released from a PC12 cell. Once the PC12 cell is stimulated by a high-concentrated K^+

solution, the depolarization of the plasma membrane may induce the influx of calcium ions (Ca^{2+}) into the cell through voltage-dependent calcium channels and the release of intracellular Ca^{2+} stores. The increase of intracellular Ca^{2+} evokes the neurotransmitter release from the cell. Besides, it was reported that stimulations by high-concentrated K^+ solutions preferentially induced the release of dopamine by exocytosis [4,18,19]. After that, the released dopamine molecules diffuse to a Nafion film and interact with $ABTS^{\bullet}$ radicals in the Nafion film on an NRC sensor. This interaction generates H^+, which will diffuse in the Nafion film, leading to the decrease of the electrical current as described previously (Figure 3a). Thus, our NRC sensor could be used to quantitatively monitor dopamine release from living cells. Furthermore, in our experiments, PC12 cells can be stored during the sensing processes without being cultured on an NRC sensor, indicating rather simple sensing processes compared with previous works [8].

Figure 3.5(b) shows the real-time changes of electrical currents in an NRC sensor by dopamine release from PC12 cells. Here, the PC12 cells were stimulated by high-concentrated K^+ solutions (containing 2.5 mM Ca^{2+}) to release dopamine by exocytosis. The graph shows that the addition of a cell suspension did not affect the electrical currents of the NRC sensor. In contrast, the additions of high-concentrated K^+ solutions caused the decrease of its electrical current, indicating that PC12 cells released a significant amount of dopamine to the buffer solution. We also measured the electrical current changes of NRC sensors in the absence of PC12 cells during the additions of different K^+ solutions, which did not show any significant current changes. These results clearly show that our sensors can selectively monitor the K^+-evoked dopamine release from live cells.

Figure 3.5(c) shows a correlation between the concentrations of released dopamine and the concentrations of K^+ solutions. The dose-response curves of our sensors (Figure 3.4(d)) were used to calculate the concentration of

dopamine released from PC12 cells. The dopamine release was increased significantly when the concentration of K^+ solutions increased from 20 to 160 mM, presumably because of the increase of membrane depolarization as reported previously [4]. This result shows that the concentration changes of extracellular K^+ may influence neurological functions such as membrane potential maintenance and neurotransmitter transport [3,4]. Previous works showed that the sensor response could be significantly delayed by the diffusion time of target molecules in solution and in Nafion layers [21]. However, in our experiment, the response time was quite quick enough for practical applications. Presumably, because of the small volume of our working solution (~10 μL), it did not take a long time for the released dopamine to reach the sensor surface. Also, H^+ generated during the sensing process can diffuse very quickly inside the Nafion film with a rather small thickness of ~200 nm, resulting in the quick response of our sensors. On the other hand, it was previously reported that the concentration of an $ABTS^{\bullet}$ radical solution (pH = 7.4) decreased by 10% after 60 min exposure to ambient air, which may cause instability of signals if the sensing experiments last for a long time period [26]. However, the rather fast response time of our sensors allowed us to finish most of the sensing experiments in less than 10 min (Figure 3.5(b)). Thus, the effect by the degradation of $ABTS^{\bullet}$ radicals is expected to be minimal in our experiments. Importantly, these results imply that our method can be used to quantitatively monitor the real-time release of biomaterials in living systems. Moreover, these results show that our method could be utilized for the real-time monitoring of living cells (Table 3.2) owing to the high sensitivity and fast responses of NRC sensors (Table 3.1).

3.5. Monitoring antipsychotic effects on K^+-evoked dopamine release from PC12 cells by NRC sensors

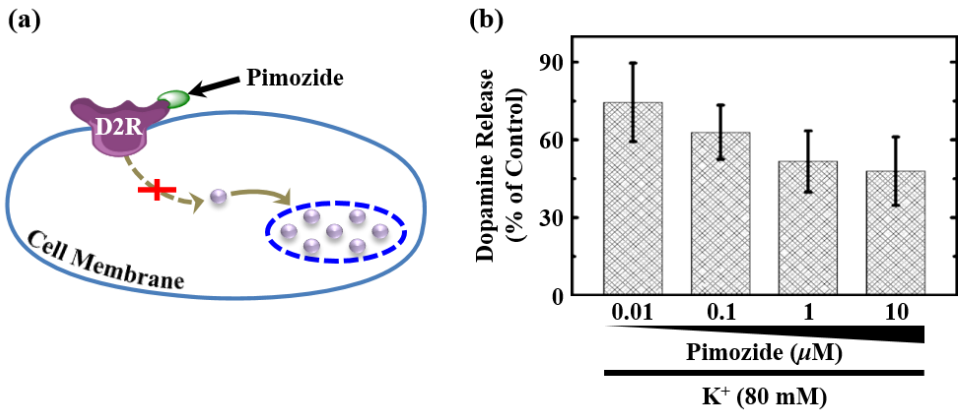

Figure 3.6. Evaluation of the effects of pimozide on K^+-evoked dopamine release from PC12 cells. (a) Schematic drawing depicting the effect mechanism of pimozide on the dopamine synthesis in PC12 cells. (b) K^+-evoked dopamine release from PC12 cells pretreated with pimozide. The bars indicate means ± SEM, (n = 4).

As the abnormal changes of dopamine levels in nervous cells are involved in neurological diseases, therapeutic methods have been suggested using dopaminergic drugs. For example, pimozide is an antipsychotic, which has been marketed to care for patients with schizophrenia [27]. Figure 3.6(a) illustrates the mechanism of the effect by pimozide for the synthesis and accumulation of dopamine in the cytosols of PC12 cells. Once pimozide molecules bind to dopamine D2 receptors (D2Rs) on a plasma membrane, their antagonistic activity inhibits the production of dopamine and the transport of dopamine vesicles [5,28]. Therefore, pimozide can induce the reduction of dopamine release from neurons and PC12 cells. Thus, by measuring the reduction of dopamine release with antipsychotic drugs via our NRC sensors, we can quantitatively evaluate the effects of antipsychotic drugs on the dopamine release.

Figure 3.6(b) shows the dependence of K^+-evoked dopamine release from PC12 cells on the concentrations of pimozide. In these experiments, PC12 cells were pretreated with pimozide with different concentrations of 0.01 - 10 μM for 24 h, followed by the stimulation of 80 mM K^+ solutions. Post-stimulated solutions were then harvested and introduced onto our NRC sensors to evaluate the released dopamine levels. The responses show that PC12 cells expressed decreasing dopamine release with higher concentrations of pimozide. It clearly shows that pimozide acted as an antagonist on D2Rs, resulting in the reduced K^+-evoked dopamine release from PC12 cells. Also, these results are consistent with reported results [5]. This indicates that our NRC sensor could be used as a reliable tool to monitor the effect of dopaminergic drugs as well as other biomedical applications.

Table 3.2. Real-time measurability of this method and previous methods for dopamine detection.

Method	**Real-time Detection**	**Cell Monitoring**	**Reference**
Electrochemistry	Yes	Yes	[18]
Graphene-FET	Yes	No data	[6]
CNT-FET	No data	No data	[7]
HPLC	Yes	No data	[22]
Electrochemistry	No data	No data	[14]
Electrochemistry	Yes	No data	[20]
CNT-FET	Yes	Yes	This work

3.6. Summary

We successfully demonstrated a biocompatible, simple, and flexible method for the effective evaluation of antipsychotic drugs on dopamine release from PC12 cells upon the stimulation of high-concentrated K^+ solutions. In this strategy, we modified floating electrode-based CNT-FET devices by a thin Nafion film containing $ABTS^{\bullet}$ radicals to build NRC sensors for dopamine detection. Using NRC sensors, we could distinguish dopamine in aqueous solutions from the concentration of 10 nM and in the presence of other neurotransmitters, indicating the sensitivity and selectivity of our method. In particular, the dopamine release from PC12 cells stimulated by high-concentrated K^+ solutions could be quantitatively monitored by our NRC sensors. Moreover, the antipsychotic effects of pimozide on the K^+-evoked dopamine release from PC12 cells were also evaluated in a concentrationdependent manner. The biocompatible capability of our method should provide a vital tool and open up various developments in biosensor research and biomedical applications.

3.7. References

[1] Ahlskog, J. E. Beating a dead horse: dopamine and Parkinson disease. *Neurology*. **2007**, *69*, 1701.

[2] Howes, O. D.; Egerton, A.; Allan, V.; McGuire, P.; Stokes, P.; Kapur, S. Mechanisms underlying psychosis and antipsychotic treatment response in schizophrenia: insights from PET and SPECT imaging. *Curr. Pharm. Des*. **2009**, *15*, 2550.

[3] Kofuji, P.; Newman, E. A. Potassium buffering in the central nervous system. *Neuroscience*. **2004**, *129*, 1045.

[4] Almaraz, L.; Gonzalez, C.; Obeso, A. Effects of high potassium on the release of [3H]dopamine from the cat carotid body in vitro. *J. Physiol.* **1986**, *379*, 293.

[5] Matsuo, T.; Izumi, Y.; Wakita, S.; Kume, T.; Takada-Takatori, Y.; Sawada, H.; Akaike, A. Haloperidol, spiperone, pimozide and aripiprazole reduce intracellular dopamine content in PC12 cells and rat mesencephalic cultures: Implication of inhibition of vesicular transport. *Eur. J. Pharmacol.* **2010**, *640*, 68.

[6] Zhang, M.; Liao, C.; Yao, Y.; Liu, Z.; Gong, F.; Yan, F. High-Performance Dopamine Sensors Based on Whole-Graphene Solution-Gated Transistors. *Adv. Funct. Mater.* **2014**, *24*, 978.

[7] Salila Vijayalal Mohan, H. K.; An, J.; Zheng, L. Sequence-dependent electrical response of ssDNA-decorated carbon nanotube, field-effect transistors to dopamine. *Beilstein J. Nanotechnol.* **2014**, *5*, 2113.

[8] Li, B. R.; Hsieh, Y. J.; Chen, Y. X.; Chung, Y. T.; Pan, C. Y.; Chen, Y. T. An ultrasensitive nanowire-transistor biosensor for detecting dopamine release from living PC12 cells under hypoxic stimulation. *J. Am. Chem. Soc.* **2013**, *135*, 16034.

[9] Park, S. J.; Song, H. S.; Kwon, O. S.; Chung, J. H.; Lee, S. H.; An, J. H.; Ahn, S. R.; Lee, J. E.; Yoon, H.; Park, T. H.; Jang, J. Human

dopamine receptor nanovesicles for gate-potential modulators in high-performance field-effect transistor biosensors. *Sci. Rep.* **2014**, *4*, 4342.

[10] Dresselhaus, M. S.; Jorio, A.; Souza Filho, A. G.; Saito, R. Defect characterization in graphene and carbon nanotubes using Raman spectroscopy. *Philos. Trans. R. Soc. A.* **2010**, *368*, 5355.

[11] Tunuguntla, R. H.; Chen, X.; Belliveau, A.; Allen, F. I.; Noy, A. High-Yield Synthesis and Optical Properties of Carbon Nanotube Porins. *J. Phys. Chem. C.* **2017**, *121*, 3117.

[12] Garcia-Leis, A.; Jancura, D.; Antalik, M.; Garcia-Ramos, J. V.; Sanchez-Cortes, S.; Jurasekova, Z. Catalytic effects of silver plasmonic nanoparticles on the redox reaction leading to $ABTS^{\bullet+}$ formation studied using UV-visible and Raman spectroscopy. *Phys. Chem. Chem. Phys.* **2016**, *18*, 26562.

[13] Patra, S.; Sene, S.; Mousty, C.; Serre, C.; Chausse, A.; Legrand, L.; Steunou, N. Design of Laccase-Metal Organic Framework-Based Bioelectrodes for Biocatalytic Oxygen Reduction Reaction. *ACS Appl. Mater. Interfaces*. **2016**, *8*, 20012.

[14] Chih, Y. K.; Yang, M. C. An 2,2'-azino-bis(3-ethylbenzthiazoline-6-sulfonic acid)-immobilized electrode for the simultaneous detection of dopamine and uric acid in the presence of ascorbic acid. *Bioelectrochemistry*. **2013**, *91*, 44.

[15] Bourbonnais, R.; Leech, D.; Paice, M. G. Electrochemical analysis of the interactions of laccase mediators with lignin model compounds. *Biochim. Biophys. Acta*. **1998**, *1379*, 381.

[16] Mohammad-Shiri, H.; Ghaemi, M.; Riahi, S.; Akbari-Sehat, A. Computational and Electrochemical Studies on the Redox Reaction of Dopamine in Aqueous Solution. *Int. J. Electrochem. Sci.* **2011**, *6*, 317.

[17] Freeman, G. B.; Mykytyn, V.; Gibson, G. E. Differential alteration of dopamine, acetylcholine, and glutamate release during anoxia and/or 3,4-diaminopyridine treatment. *Neurochem. Res.* **1987**, *12*, 1019.

[18] Abe, H.; Ino, K.; Li, C. Z.; Kanno, Y.; Inoue, K. Y.; Suda, A.; Kunikata, R.; Matsudaira, M.; Takahashi, Y.; Shiku, H.; Matsue, T. Electrochemical Imaging of Dopamine Release from Three-Dimensional-Cultured PC12 Cells Using Large-Scale Integration-Based Amperometric Sensors. *Anal. Chem.* **2015**, *87*, 6364.

[19] Kumar, G. K.; Overholt, J. L.; Bright, G. R.; Hui, K. Y.; Lu, H.; Gratzl, M.; Prabhakar, N. R. Release of dopamine and norepinephrine by hypoxia from PC-12 cells. *Am. J. Physiol.* **1998**, *274*, C1592.

[20] Chen, P. Y.; Vittal, R.; Nien, P. C.; Ho, K. C. Enhancing dopamine detection using a glassy carbon electrode modified with MWCNTs, quercetin, and Nafion. *Biosens. Bioelectron.* **2009**, *24*, 3504.

[21] Chang, K. M.; Chang, C. T.; Chan, K. M. Development of an ion sensitive field effect transistor based urea biosensor with solid state reference systems. *Sensors (Basel)*. **2010**, *10*, 6115.

[22] De Benedetto, G. E.; Fico, D.; Pennetta, A.; Malitesta, C.; Nicolardi, G.; Lofrumento, D. D.; De Nuccio, F.; La Pesa, V. A rapid and simple method for the determination of 3,4-dihydroxyphenylacetic acid, norepinephrine, dopamine, and serotonin in mouse brain homogenate by HPLC with fluorimetric detection. *J. Pharm. Biomed. Anal.* **2014**, *98*, 266.

[23] Kim, B.; Lee, J.; Namgung, S.; Kim, J.; Park, J. Y.; Lee, M. S.; Hong, S. DNA Sensors based on CNT-FET with Floating Electrodes. *Sensor. Actuator. B Chem.* **2012**, *169*, 182.

[24] Lee, M.; Lee, J.; Kim, T. H.; Lee, H.; Lee, B. Y.; Park, J.; Jhon, Y. M.; Seong, M. J.; Hong, S. 100 nm scale low-noise sensors based on aligned

carbon nanotube networks: overcoming the fundamental limitation of network-based sensors. *Nanotechnology*. **2010**, *21*, 055504.

[25] Bai, O.; Wei, Z.; Lu, W.; Bowen, R.; Keegan, D.; Li, X. M. Protective effects of atypical antipsychotic drugs on PC12 cells after serum withdrawal. *J. Neurosci. Res.* **2002**, *69*, 278.

[26] Ozgen, M.; Reese, R. N.; Tulio, A. Z., Jr.; Scheerens, J. C.; Miller, A. R. Modified 2,2-azino-bis-3-ethylbenzothiazoline-6-sulfonic acid (ABTS) method to measure antioxidant capacity of Selected small fruits and comparison to ferric reducing antioxidant power (FRAP) and 2,2'-diphenyl-1-picrylhydrazyl (DPPH) methods. *J. Agric. Food. Chem.* **2006**, *54*, 1151.

[27] Mothi, M.; Sampson, S. Pimozide for schizophrenia or related psychoses. *Cochrane Database Syst. Rev.* **2013**, CD001949.

[28] Binda, A. V.; Kabbani, N.; Levenson, R. Regulation of dense core vesicle release from PC12 cells by interaction between the D2 dopamine receptor and calcium-dependent activator protein for secretion (CAPS). *Biochem. Pharmacol.* **2005**, *69*, 1451.

Chapter 4. Modified floating electrode-based sCNT transistors for the evaluation of anti-inflammatory effects via TNFα secretion from Raw 264.7 cells

4.1. Introduction

Inflammatory bowel disease (IBD) is a serious chronic gastrointestinal disorder which may be caused by the abnormal activation of the nuclear factor κB (NF-κB) pathway [1,2]. This abnormal activation increases the production and secretion of pro-inflammatory cytokines including tumor necrosis factor α (TNFα). Previous studies have shown that TNFα plays a crucial role in the pathogenesis of IBD; therefore, the estimation of TNFα levels is important in the diagnosis and therapy of IBD [3,4]. For example, the average TNFα levels in the blood of healthy donors and patients with Crohn's disease-a type of IBD-were about 3 and 6 ng/L, respectively [5]. Moreover, anti-TNF agents have been widely used in the treatment of IBD [6].

Labeling methods, such as ELISA technique, flow cytometry and polymerase chain reaction have been used for the detection of TNFα and other markers with a high sensitivity [7-9]. However, these methods often require complex equipment and time-consuming preparatory procedures. Recently, FET-immunosensors have been considered as a potential candidate for the detection and quantification of inflammation-related cytokines [10-12]. Even though the immunosensors are usually disposable devices because of the formation of stable immune complexes, they have exhibited specific, rapid, and real-time responses by the small volume of samples[13,14]. However, their applications for the monitoring of drug effects related with clinical diseases are still limited.

Herein, we developed a modified floating electrode-based CNT-FET sensor for the quantitative monitoring of drug effects on cytokines related

with IBD (Figure 4.1). In this work, antibody (anti-TNFα) molecules were immobilized on the floating electrodes of a CNT-FET sensor to build a TNF sensor which can detect TNFα at various concentrations via a specific interaction between TNFα and anti-TNFα molecules. In this sensor, floating electrode structures enhanced the sensor sensitivity, and also, their gold surface could be easily functionalized to build selective sensors [15].

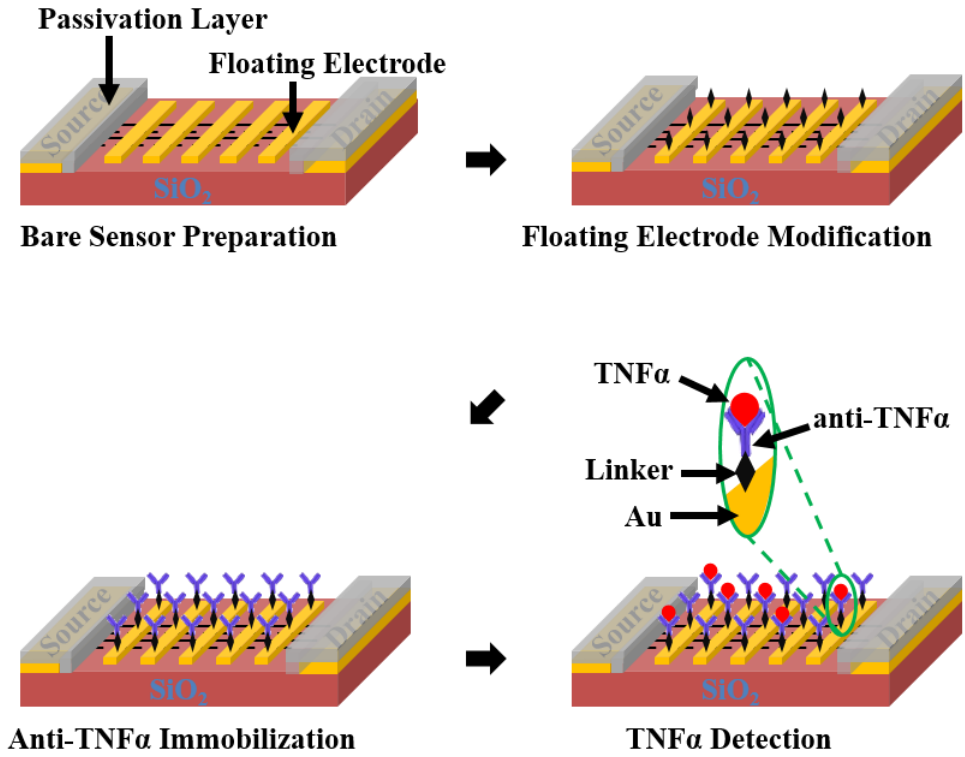

Figure 4.1. Schematic diagram depicting the preparatory procedure of TNF sensors for TNFα detection.

Our TNF sensor recognized TNFα from other IBD-related cytokines such as interleukin-1β (IL-1β) and interleukin-6 (IL-6) with a quick response at a low concentration down to 1 pg/L. Using this method, we could quantitatively monitor the effect of an anti-inflammatory agent, lupeol, on the production and secretion of the pro-inflammatory cytokine, TNFα, from Raw 264.7 cells. The results indicate that lupeol inhibits the TNFα production of LPS-

stimulated Raw 264.7 cells as previously reported [7]. This method exploits the advantages of floating electrode-based sensor structures such as high sensitivity and label-free simple detection, and it has the potential for monitoring other biomaterials of clinical interests simply by using different antibodies. Thus, our novel strategy can be a powerful tool for various basic biomedical research and clinical applications.

4.2. Characteristics of TNF sensors

To confirm the formation of anti-TNF*α* molecules on gold floating electrodes, the topography images of a sensor device were taken using an AFM system.

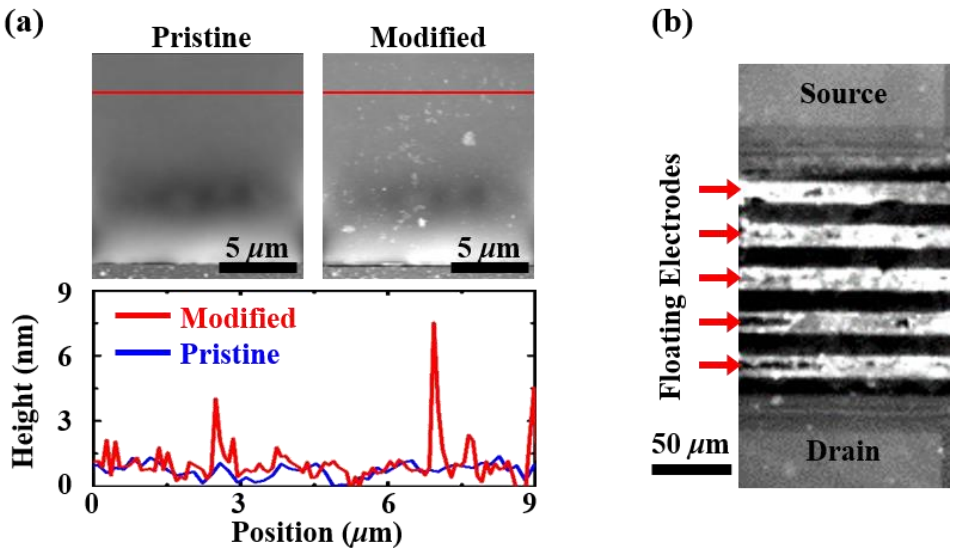

Figure 4.2. Characterization of a TNF sensor based on a CNT-FET sensor with floating electrodes. (a) AFM images (top) of the surface of a floating electrode before (left) and after (right) anti-TNFα immobilization and height profile comparison (bottom) of that surface before (blue) and after (red) the immobilization. (b) Fluorescence image of a TNF sensor obtained after the incubation of the sensor with Alexa Fluor 488-conjugated anti-rabbit IgG.

Figure 4.2(a) shows the AFM images of a floating electrode surface before and after the modification with anti-TNF*α*. First, the bare surface of a gold floating electrode was imaged, and then, the surface was functionalized with anti-TNF*α*. Successively, the topography image of the gold electrode surface was taken at the same position and condition. The images show the spots on the gold electrode after the modification with the size at a nanometer level which is consistent with the size of a single protein molecule [16]. The

comparison of height profiles shows a height increase by the presence of anti-TNFα molecules, indicating the successful immobilization of the anti-TNFα molecules on the floating electrodes. In our sensors, the floating electrodes play the role of substrates for the immobilization of anti-TNFα. Furthermore, floating electrode structures improve the sensitivity of biosensors, resulting from the increased number of Schottky barriers [15].

We also performed a fluorescent assay to confirm the bioactivity of anti-TNFα on floating electrodes. Figure 4.2(b) shows the fluorescent image of a sensor stained with fluorescent dye-conjugated anti-rabbit IgG. Note that, the fluorescent signals appeared only on the regions of floating electrodes. Because anti-rabbit IgG was specific for rabbit clonal anti-TNFα, this result indicates that anti-TNFα molecules were successfully immobilized only on the floating electrodes. Furthermore, it also implies that the bioactivity of anti-TNFα was not affected by the immobilizing procedure.

4.3. Detection of TNFα by using TNF sensors

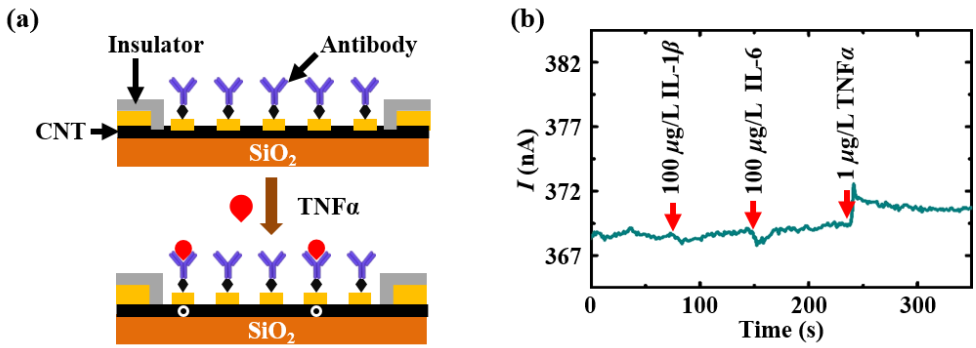

Figure 4.3. Responses of TNF sensors to the addition of cytokine solutions. (a) Schematic diagram showing the sensing mechanism of a TNF sensor. (b) Real-time response of a TNF sensor to various pro-inflammatory cytokines such as IL-1β, IL-6 and TNFα.

Figure 4.3(a) illustrates the sensing mechanism of our sensor for the detection of TNF*α*. When TNF*α* was introduced on the surface of a sensor, TNF*α* specifically interacted with anti-TNF*α* immobilized on the floating electrodes. Previous reports have shown that antibody-antigen interactions could raise the metal work function of floating electrodes, resulting in the decrease of Schottky barrier height (Figure 1.3(b)) [17]. Therefore, the hole carrier transport from the electrode to the sCNT increased, which should induced the conductance increase in underlying *p*-type semiconducting channels like the *p*-type sCNT channels in our TNF sensor (Figure 1.6) [10-12]. By measuring the electrical current changes of TNF sensors, the levels of TNF*α* could be quantitatively evaluated.

Figure 4.3(b) shows the real-time responses of a TNF sensor to various pro-inflammatory cytokines such as IL-1*β*, IL-6 and TNF*α* which are largely produced in IBD [3,18]. During the addition of IL-1*β* and IL-6, there were no significant changes in electrical currents in the TNF sensor. Note that, IL-1*β* and IL-6 were added at a rather high concentration of 100 *μ*g/L, whereas the

addition of a relatively low 1 μg/L concentration of TNFα caused the sharp increase of the electrical currents. Moreover, the size of IL-1β is quite equivalent with that of TNFα. It clearly shows that the TNF sensor responded to TNFα without being disturbed by other cytokines. This result also implies that our TNF sensors could be applied as selective biosensors for the detection of cytokines related with IBD.

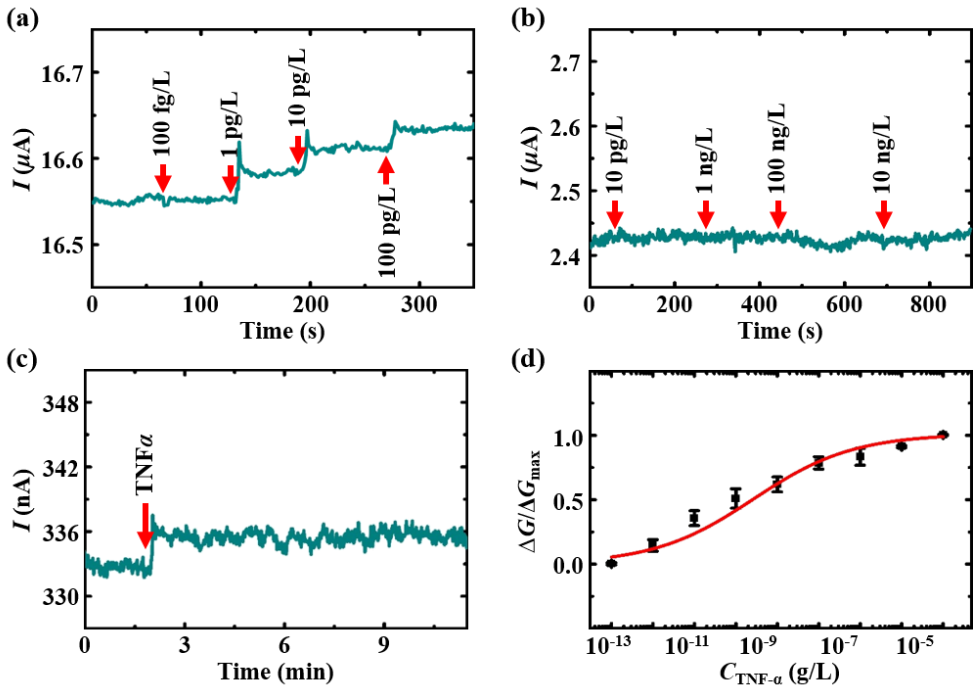

Figure 4.4. Real-time measurements of electrical currents in sensors in response to the addition of TNFα solutions. (a) Real-time electrical current changes of a TNF sensor during the addition of TNFα solutions. (b) Responses of a CNT-FET sensor with pristine floating electrodes during the addition of various TNFα concentrations. (c) Real-time electrical current measurement of a TNF sensor in response to the addition of a TNFα solution for 10 min. (d) Dose-dependent relative conductance changes of TNF sensors in response to the concentration changes of TNFα. Data are expressed as means ± SEM (n = 3).

Sensors immobilized with anti-TNFα were utilized to detect various concentrations of TNFα solutions. Figure 4.4(a) shows the real-time electrical current changes of a sensor during the addition of TNFα solutions with a concentration range of 100 fg/L to 100 pg/L. During the sensing measurements, a source-drain bias voltage of 0.1 V was applied on the sensors. The currents in the sensor increased immediately when a TNFα solution was introduced. Such quick and real-time responses are one of the main advantages of FET-based sensors, which have been reported by many other groups [10,14,15,19-21]. Note that when the sensor was exposed to a TNFα solution with 1 pg/L or higher concentrations, it exhibited current changes much larger than noise amplitudes. For example, electrical currents in the sensor increased 32, 61, and 83 nA during the addition of TNFα solutions at concentrations of 1, 10, and 100 pg/L, respectively. It implies that our sensor can be utilized as a highly-sensitive sensor for the TNFα detection. Here, similar signals were obtained even when TNFα solutions with various concentrations were added to different sensors separately. Because TNFα levels in the human blood were reported to be about 3 ng/L, these results show that our TNF sensors have a sensitivity high enough for the monitoring of TNFα levels in clinical samples [5]. On the other hand, there were no significant changes in the electrical currents of an unmodified floating electrode-based CNT-FET sensor by the addition of TNFα solutions (Figure 4.4(b)). Moreover, electrical currents in a TNF sensor were monitored for 10 min to test the long-term stability of the sensor signal (Figure 4.4(c)). The currents in the sensor increased and gradually stabilized after the addition of a TNFα solution. These results clearly show that the signals of our sensors were caused by the interaction between TNFα and anti-TNFα molecules on the floating electrodes of our sensors.

A dose-dependent curve presented in Figure 4.4(d) was obtained by converting the current changes of sensors to normalized conductance changes

($\Delta G/\Delta G_{max}$), which is defined as the conductance change ratio over the maximum conductance change of the sensor. We performed the sensing experiments with different sensor chips for statistical analysis. The relative conductance change increased as the concentration of TNFα increased, and it saturated at around 1 μg/L of TNFα. Note that the error bars were much smaller than the sensor signals $\Delta G/\Delta G_{max}$ from 1 pg/L of TNFα, indicating the high sensitivity and reliability of our sensors. Moreover, the dose-dependent curve was also analyzed by a Hill equation for the quantification of TNFα levels (red solid line in Figure 4.4(d)).

4.4. Monitoring the effect of anti-inflammatory on the NF-κB signaling pathway

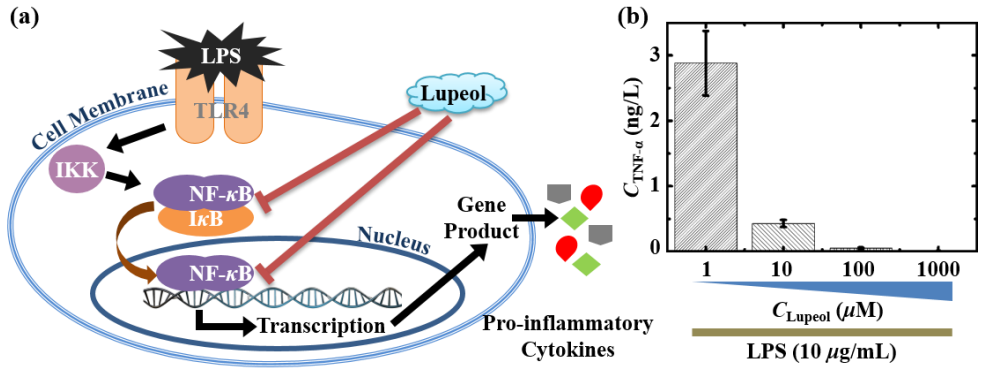

Figure 4.5. Evaluation of the inhibiting effect of lupeol on the LPS-induced NF-κB signaling pathway. (a) Schematic drawing depicting the inhibition mechanism of lupeol on the LPS-induced TNFα secretion in mouse macrophages. (b) Concentration dependence of TNFα secreted from Raw 264.7 cells on the concentrations of lupeol under the stimulation of LPS.

The NF-κB signaling pathway has been found to be a key regulator in IBD, and thus, the therapeutic method of IBD has been recently suggested using inhibitors blocking this pathway [7,22]. Figure 4.5(a) illustrates the inhibition mechanism for the NF-κB signaling pathway by lupeol which may be a strong anti-inflammatory and anti-cancer agent. A previous report showed that lupeol inhibited the DNA binding via the suppression of the phosphorylation and degradation of IκBα which was required for the activation of the NF-κB signaling pathway. Consequently, lupeol could strongly suppress the production and secretion of LPS-induced pro-inflammatory cytokines including TNFα in mouse macrophages [7,23,24]. Here, our TNF sensors were utilized to monitor the effect of lupeol on the activation of the NF-κB signaling pathway in the Raw 264.7 cell line via the estimation of TNFα levels.

Figure 4.5(b) shows the dependence of LPS-induced TNFα levels on the different concentrations of lupeol. In this experiment, we pretreated Raw 264.7 cells with lupeol at concentrations in the range of 1 - 1000 μM for 24 h, followed by the stimulation of 10 μg/mL LPS for 2 h. Medium solutions were then harvested and introduced onto a TNF sensor to quantify the level of TNFα. To quantitatively estimate the inhibition of lupeol on the NF-κB pathway, electric current changes were converted to the concentrations of TNFα using the dose-dependent curve fitted in Figure 4.4(d). When Raw 264.7 cells were pretreated with lupeol, the TNFα production significantly decreased. This clearly indicates that lupeol acted as an inhibitor on Raw 264.7 cells, blocking the production and secretion of TNFα. Moreover, the results are consistent with the previous works performed by our group via the ELISA method [7]. Furthermore, this result clearly shows that the TNF sensor could be used as a highly sensitive tool to monitor the effect of versatile drugs related with IBD and other diseases.

4.5. Summary

We report a modified floating electrode-based sensor as a simple but effective method for the quantitative evaluation of drugs related with IBD. In this method, floating electrode-based CNT-FET sensors were modified by anti-TNFα, enabling the selective and quantitative monitoring of TNFα among other inflammatory cytokines related with IBD. Our TNF sensors exhibited a high sensitivity to TNFα with the detection limit of 1 pg/L. Importantly, the TNF sensors could be utilized to evaluate the inhibiting effects of lupeol, an anti-inflammatory agent, on the NF-κB signaling pathway via the monitoring of TNFα secretion from Raw 264.7 cells under LPS stimulation. Because our method can be applied to rapidly and accurately monitor biomaterials of clinical interests, it should open versatile biomedical applications such as drug screening and inflammation monitoring.

4.6. References

[1] Abraham, C.; Cho, J. H. Inflammatory bowel disease. *N. Engl. J. Med.* **2009**, *361*, 2066.

[2] Barnes, P. J.; Karin, M. Nuclear factor-kappaB: a pivotal transcription factor in chronic inflammatory diseases. *N. Engl. J. Med.* **1997**, *336*, 1066.

[3] Neurath, M. F. Cytokines in inflammatory bowel disease. *Nat. Rev. Immunol.* **2014**, *14*, 329.

[4] Schreiber, S.; Nikolaus, S.; Hampe, J. Activation of nuclear factor kappa B inflammatory bowel disease. *Gut*. **1998**, *42*, 477.

[5] Gutierrez, A.; Frances, R.; Amoros, A.; Zapater, P.; Garmendia, M.; Ndongo, M.; Cano, R.; Jover, R.; Such, J.; Perez-Mateo, M. Cytokine association with bacterial DNA in serum of patients with inflammatory bowel disease. *Inflamm. Bowel. Dis.* **2009**, *15*, 508.

[6] Nielsen, O. H.; Ainsworth, M. A. Tumor necrosis factor inhibitors for inflammatory bowel disease. *N. Engl. J. Med.* **2013**, *369*, 754.

[7] Lee, C.; Lee, J. W.; Seo, J. Y.; Hwang, S. W.; Im, J. P.; Kim, J. S. Lupeol inhibits LPS-induced NF-kappa B signaling in intestinal epithelial cells and macrophages, and attenuates acute and chronic murine colitis. *Life Sci.* **2016**, *146*, 100.

[8] Bueno, C.; Rodriguez-Caballero, A.; García-Montero, A.; Pandiella, A.; Almeida, J.; Orfao, A. A new method for detecting TNF-α-secreting cells using direct-immunofluorescence surface membrane stainings. *J. Immunol. Methods*. **2002**, *264*, 77.

[9] Komatsu, M.; Kobayashi, D.; Saito, K.; Furuya, D.; Yagihashi, A.; Araake, H.; Tsuji, N.; Sakamaki, S.; Niitsu, Y.; Watanabe, N. Tumor necrosis factor-alpha in serum of patients with inflammatory bowel disease as measured by a highly sensitive immuno-PCR. *Clin. Chem.* **2001**, *47*, 1297.

[10] Pui, T. S.; Agarwal, A.; Ye, F.; Huang, Y.; Chen, P. Nanoelectronic detection of triggered secretion of pro-inflammatory cytokines using CMOS compatible silicon nanowires. *Biosens. Bioelectron.* **2011**, *26*, 2746.

[11] Zhang, Y.; Chen, R.; Xu, L.; Ning, Y.; Xie, S.; Zhang, G. J. Silicon nanowire biosensor for highly sensitive and multiplexed detection of oral squamous cell carcinoma biomarkers in saliva. *Anal. Sci.* **2015**, *31*, 73.

[12] Nam, H.; Oh, B. R.; Chen, P.; Chen, M.; Wi, S.; Wan, W.; Kurabayashi, K.; Liang, X. Multiple MoS2 Transistors for Sensing Molecule Interaction Kinetics. *Sci. Rep.* **2015**, *5*, 10546.

[13] Moina, C.; Ybarr, G. Fundamentals and Applications of Immunosensors. In *Advances in Immunoassay Technology*; Chiu, N., Ed.; InTechOpen, 2012; pp 65.

[14] de Moraes, A.; Kubota, L. Recent Trends in Field-Effect Transistors-Based Immunosensors. *Chemosensors*. **2016**, *4*, 20.

[15] Kim, B.; Lee, J.; Namgung, S.; Kim, J.; Park, J. Y.; Lee, M. S.; Hong, S. DNA sensors based on CNT-FET with floating electrodes. *Sens. Actuators B: Chem.* **2012**, *169*, 182.

[16] Erickson, H. P. Size and shape of protein molecules at the nanometer level determined by sedimentation, gel filtration, and electron microscopy. *Biol. Proced. Online*. **2009**, *11*, 32.

[17] Kim, S. N.; Rusling, J. F.; Papadimitrakopoulos, F. Carbon Nanotubes for Electronic and Electrochemical Detection of Biomolecules. *Adv. Mater.* **2007**, *19*, 3214.

[18] Atreya, I.; Atreya, R.; Neurath, M. F. NF-kappaB in inflammatory bowel disease. *J. Intern. Med.* **2008**, *263*, 591.

[19] Lee, M.; Lee, J.; Kim, T. H.; Lee, H.; Lee, B. Y.; Park, J.; Jhon, Y. M.; Seong, M. J.; Hong, S. 100 nm scale low-noise sensors based on aligned

carbon nanotube networks: overcoming the fundamental limitation of network-based sensors. *Nanotechnology*. **2010**, *21*, 055504.

[20] Jin, H. J.; An, J. M.; Park, J.; Moon, S. J.; Hong, S. "Chemical-pain sensor" based on nanovesicle-carbon nanotube hybrid structures. *Biosens. Bioelectron.* **2013**, *49*, 86.

[21] Kim, T. H.; Lee, B. Y.; Jaworski, J.; Yokoyama, K.; Chung, W. J.; Wang, E.; Hong, S.; Majumdar, A.; Lee, S. W. Selective and sensitive TNT sensors using biomimetic polydiacetylene-coated CNT-FETs. *ACS Nano*. **2011**, *5*, 2824.

[22] Seo, J. Y.; Lee, C.; Hwang, S. W.; Chun, J.; Im, J. P.; Kim, J. S. Nimbolide Inhibits Nuclear Factor-capital KA, CyrillicB Pathway in Intestinal Epithelial Cells and Macrophages and Alleviates Experimental Colitis in Mice. *Phytother. Res.* **2016**, *30*, 1605.

[23] Sharif, O.; Bolshakov, V. N.; Raines, S.; Newham, P.; Perkins, N. D. Transcriptional profiling of the LPS induced NF-kappaB response in macrophages. *BMC Immunol.* **2007**, *8*, 1.

[24] Kang, C. C.; Chuang, Y. J.; Tung, K. C.; Chao, C. C.; Tang, C. Y.; Peng, S. C.; Wong, D. S. A genetic algorithm-based Boolean delay model of intracellular signal transduction in inflammation. *BMC Bioinformatics*. **2011**, *12 Suppl 1*, S17.

Chapter 5. Conclusions

In this dissertation, biosensors based on sCNT transistors with floating electrodes were successfully developed for the real-time monitoring cellular transport such as Ca^{2+} influx, dopamine and TNFα release for living cells. Interestingly, the biosensors could be utilized to quantitatively evaluate the effects of drugs on the cellular transport of the cells. Such quantitative evaluation capability of our method should provide a versatile tool for biomedical studies and clinical applications such as drug screening.

Firstly, reusable sensors were developed based on sCNT transistors for the effect evaluation of antihistamine drugs via the real-time monitoring of histamine-induced Ca^{2+} influx into HeLa cells. By using a single reusable sensor, the electrophysiological responses of individual HeLa cells to various concentrations of histamine could be quantitatively monitored. Moreover, the effects of antihistamine drugs such as cetirizine and chlorphenamine were also quantitatively evaluated via the real-time monitoring of histamine-induced Ca^{2+} influx using reusable sensors. Significantly, this method allows us to eliminate the errors from device-to-device variations, resulting in statistically meaningful results.

Next, sCNT transistors were coated with hybrid films containing Nafion and $ABTS^{\bullet}$ radicals to build biosensors for the effect evaluation of antipsychotic drugs via the real-time monitoring of K^{+}-evoked dopamine release from PC12 cells. The biosensors could distinguish dopamine from other neurotransmitters such as glutamate and acetylcholine with a detection limit down to 10 nM. These results indicate the high selectivity and high sensitivity of our biosensors, which allows us to apply the biosensors for the real-time monitoring of dopamine release from PC12 cells stimulated by high concentration K^{+} solutions. Significantly, our method could be also utilized

to quantitatively evaluate the effects of pimozide, an antipsychotic drug, on dopamine release from stimulated PC12 cells.

Additionally, sCNT transistors with floating electrodes modified by anti-TNFα were reported as selective and sensitive TNF sensors for the effect evaluation of anti-inflammatory drugs via the quantification of TNFα levels. The specific interactions between TNFα and anti-TNFα immobilized on the floating electrodes resulted in the TNFα detectability of the TNF sensors at a low concentration of 1 pg/L even in the presence of other cytokines such as IL-1β and IL-6. Moreover, the high selectivity and high sensitivity of the TNF sensors also allowed us to quantitatively evaluate the anti-inflammatory effects of lupeol via the monitoring of TNFα levels secreted from LPS-stimulated Raw 264.7 cells.

Acknowledgement

This dissertation has been completed under the grand support and impressive assistance of my advisor, members at HND laboratory (SNU) and my family.

First of all, I would like to give many thanks to my advisor, Professor Seunghun Hong, who has supported me a lot since I came to Korea for my Ph. D study. I think I am extremely lucky having an erudite advisor. The valuable guidance and advice of Professor Hong on my study help me to significantly improve skills in regard to scientific research and paper writing, which are beneficial to my future. Beside my advisor, I would also like to acknowledge other professors in my graduation committee for their insightful comments on my dissertation.

In additional, I appreciate the assistance of all members at HND laboratory for me in performing experiments and living in Korea. Dr. Van-Thao Ta brought a chance to study in Korea to me. Dr. Shashank Shekhar is a kind and enthusiastic man. Dr. Dong-guk Cho, who trained me to use equipment in our lab, often gives many good ideas. Dr. Daesan Kim is a high tech and funny man. Dr. Jeongsu Kim, who can play many kind of games, enthusiastically helped me in using AFM machine. Dr. Duckhyung Cho is a gentle and friendly lab-leader. Dr. Minju Lee is an accommodating and hard working person. Dr. Myungjae Yang, an intelligent guy, is always willing to help others. Haneul Yoo assisted me a lot in my graduation. Narae Shin usually genuinely cares about everyone in the lab. Youngtak Cho is a generous gym guy, who often helped me to order materials and chemicals. Joonghyun Shin is a nice neighbor, who aided me in understanding many documents in Korean. Jin-Young Jeong, who carefully writes lab notes, helped me to maintain the survival of cell lines. Inkyoung Park has many good and difficult questions. Jeehye Park and Hyesong Jeon are pleasant girls.

Last but not the least, I would like to express my gratitude to my parents and my appreciation to my lovely wife and my little boy. All my family members always stand by and encourage me throughout my Ph. D study. Moreover, I would like to thank my Vietnamese friends at SNU, who make me feel happy and not alone when I live far away from my family.

(*In Vietnamese*) Tôi muốn gửi lời cảm ơn chân thành tới gia đình và bạn bè, những người luôn ở bên và giúp đỡ tôi trong suốt thời gian qua. Điều đó đã tạo điều kiện giúp tôi tự tin trong cuộc sống sinh hoạt và học tập nghiên cứu tại Đại học Quốc gia Seoul, Hàn Quốc. Tôi đã nhận được rất nhiều sự quan tâm, động viên và khích lệ đặc biệt là từ bố, mẹ, vợ và con trai trong quá trình hoàn thành luận án này. Con cảm ơn bố mẹ; cảm ơn vợ và con trai.

2019. 06. 28

Pham Ba Viet Anh